electronics

MDPI

Article

Intrinsic Regularity Analysis and Optimization Control of Current Stress and RMS for Dual-Active Bridge Converter

Laiyong Zhang *, Chunming Tu, Fan Xiao, Bei Liu and Peiqiang Li

National Electric Power Conversion and Control Engineering Technology Research Center, Hunan University, Changsha 410082, China; chunming_tu@263.net (C.T.); woliaokk321@hnu.edu.cn (F.X.); beiliu@hnu.edu.cn (B.L.); lpqcs@hnu.edu.cn (P.L.)

* Correspondence: laiyongzhang@hnu.edu.cn

Abstract: Currently, current stress optimization control and current effective value optimization control have become the mainstream methods for real-time optimization control of dual-active bridge converters. However, there is still a lack of systematic research on the internal optimization regularities between the two and their respective internal optimization regularities, as well as problems such as the complex derivation of the effective value optimization control variable function. To address these issues, this paper analyzes the optimization results of stress optimization, effective value optimization, and double-objective entropy weight method optimization, and it explores the regularities and connections between the optimization variables of three optimizations in different power segments in different local optimal modes. Based on these regularities, the trigonometric function polar coordinate method is innovatively employed to derive the function expression of the RMS optimization control variable. Firstly, the four local optimal modes obtained from existing research are optimized by double-objective optimization. According to the weight settings, the optimization results of stress optimization, effective value optimization, and double-objective entropy weight method optimization are obtained. Subsequently, the optimization results are analyzed and compared, and the regularities between the optimization variables of these four local modes in different power segments under three optimizations are derived. Then, based on these regularities, the function expressions of the minimum current stress and the minimum effective value, as well as the function expressions of the optimized control variables, are derived by using the trigonometric function polar coordinate method. Finally, by comparing the current stress values and effective values of these four local optimal modes in the full power range, the global optimal mode and global optimal control variables in this range are selected, thereby achieving real-time global optimal control under power or voltage fluctuations. Simulations and experiments confirm the correctness of the theoretical analysis and the effectiveness of the optimization control strategy.

Keywords: dual active bridge DC/DC converter; double-objective optimization; local optimal working mode; global optimal working mode; trigonometric function polar coordinate method

check for updates

Citation: Zhang, L.; Tu, C.; Xiao, F.; Liu, B.; Li, P. Intrinsic Regularity Analysis and Optimization Control of Current Stress and RMS for Dual-Active Bridge Converter. *Electronics* **2024**, *13*, 4802. https://doi.org/10.3390/electronics13234802

Academic Editor: Fabio Corti

Received: 4 November 2024
Revised: 28 November 2024
Accepted: 3 December 2024
Published: 5 December 2024

Copyright: © 2024 by the authors. Licensee MDPI, Basel, Switzerland. This article is an open access article distributed under the terms and conditions of the Creative Commons Attribution (CC BY) license (https://creativecommons.org/licenses/by/4.0/).

1. Introduction

With increasingly serious problems such as energy crises and environmental pollution, the development of green energy has become particularly urgent. Among them, the grid-connection of photovoltaic and wind energy, the large-scale use of electric vehicles, and the application of smart DC distribution networks all require more advanced and efficient power conversion and control devices [1–3]. As one of the devices for power conversion and control, the dual-active bridge (DAB) DC–DC converter has received widespread attention due to its ability to connect different voltage levels and effectively regulate power and voltage. With advantages such as symmetrical structure, bidirectional energy flow, electrical isolation, high power density, and ease of achieving soft switching, the DAB has become a focal point of research in DC power conversion equipment [1–4].

The efficiency optimization of the DAB converter has always been a research hotspot and difficulty. With the application of advanced switching devices and new high-frequency transformers, the research focus of DAB converter efficiency optimization has shifted to modulation method optimization and optimization target selection. The modulation method has been developed from traditional single-phase shift (SPS), extended phase shift (EPS), and double-phase shift (DPS) to triple-phase shift (TPS), and the optimization target has developed from stress optimization and reactive power optimization to effective value (RMS) optimization [5–8], which are shown in Figure 1. The combination of the modulation method and optimization objective has become a key factor in improving its efficiency and has become one of the hotspots of current research. Among them, the optimization of current stress, reactive power, and RMS value in TPS modulation have received widespread attention and in-depth research due to their three control degrees of freedom, which can better optimize efficiency [9–12].

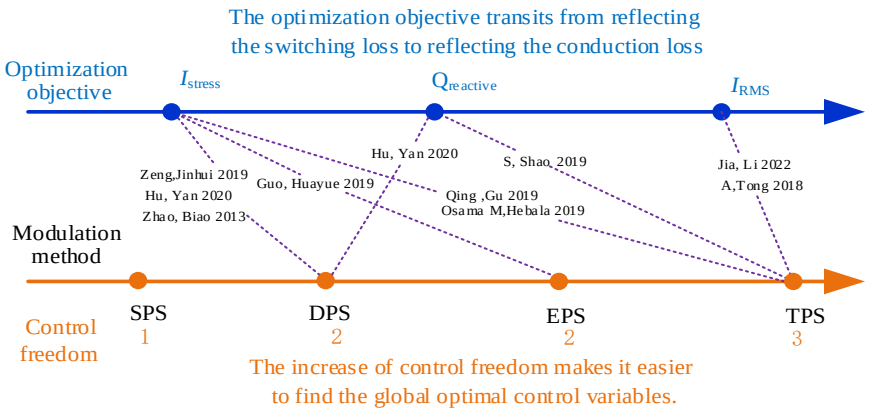


Figure 1. The evolution process of modulation methods and optimization objectives, where Zeng, Jinhui 2019, Hu, Yan 2020, Zhao, Biao 2013, Guo, Huayue 2019, Qing, GU 2019, Osama M, Hebala 2019, S, Shao 2019, Jia, Li 2022 and A, Tong 2018 are from Refs. [5–8,10,13–16] respectively.

Currently, there has been extensive research on the DAB in areas such as mode classification, equivalent simplification, and stress optimization. However, there are still deficiencies in summarizing the rules between optimization variables, the mathematical derivation of the optimization control variable function, and the comparison of the optimization effects of different optimization objectives. In terms of mode classification and rule summary, [9,10,15] classifies DAB modes effectively, but these works lack a systematic summary of the rules among optimization variables, resulting in extremely complex derivation of the optimization control variable function, which needs to be further improved. In terms of optimization algorithms, stress optimization, or reactive power optimization, in [9,10,17,18] the authors employ the KKT (Karush–Kuhn–Tucker) conditions to solve for the global optimal solution. However, the prerequisite for using this method is that both the objective function and the constraint conditions must be convex functions, which can be complex to prove or difficult to satisfy. In terms of comparing different optimization objectives, Ref. [13] compares the reactive power optimization and stress optimization. However, this comparison was conducted under dual-phase shift (DPS) modulation rather than triple-phase shift (TPS) modulation, failing to fully utilize the three degrees of freedom for optimization. Currently, there is no comparison between stress optimization and RMS optimization under TPS modulation. Ref. [16] establishes a model based on decomposing the inductor current waveform into multiple standard triangular waves and seeks to find the minimum RMS current value for the corresponding transmission power by establishing a global optimal condition equation. However, the derivation process of this method is excessively cumbersome and complex.

In view of the deficiencies in previous studies, this paper first selects four local optimal modes with the characteristics of low stress or RMS value under the same transmission

power in different power segments from 12 modes in the DAB [10,19], and the research models them in the time domain. Based on this, the Pareto solution is obtained through double-objective optimization of the current stress and RMS value. Then, the optimization results of stress optimization, RMS optimization, and double-objective entropy weight method optimization are obtained by setting different weights for the Pareto solution. Subsequently, the three optimization results are analyzed and compared to determine the optimization variable regularities in the different power segments of different modes. Then, based on the regularities, the function expressions of the minimum stress and the minimum RMS value, as well as the corresponding optimization control variables, are derived by using the power constraint condition and the trigonometric function polar coordinate method. Finally, by comparing the stress and RMS values of different local optimal modes, the corresponding global optimal mode and global optimal control variables are selected. The specific innovations are as follows:

(1) Double-objective optimization is applied to four local optimal modes to obtain the Pareto solution, and then different weights are assigned to obtain the optimization results of three different optimizations. Based on the optimization results, the regularities among the optimization variables of different power segments in each local optimal mode under these three optimizations are analyzed. Through further comparison and analysis of these regularities, the inherent regularities and relationships between stress optimization and RMS optimization are revealed.

(2) Based on the regularities among the optimization variables, the function expression for the RMS optimization control variable is derived using trigonometric function polar coordinate methods. By comparing the RMS values of these four local optimal modes, the global optimal mode and global optimal control variable for RMS optimization are selected in the full power range. On this basis, the comprehensive global optimal mode is obtained by combining the global optimal mode for stress.

2. Classification of DAB Operating Modes and Main Parameters

According to the power flow and port voltage ratio of the DAB, its operating conditions can be divided into six categories [10,19]; mainly, these include the following:

1. Forward/Matched ($k = 1$)
2. Reverse/Matched ($k = 1$)
3. Forward/ Buck ($k < 1$)
4. Reverse/ Buck ($k < 1$)
5. Forward/ Boost ($k > 1$)
6. Reverse/ Boost ($k > 1$)

The output voltage V_o is converted to the input side to obtain nV_o, as shown in Figure 2. The ratio of nV_o to the input voltage V_i is defined as the voltage regulation ratio k, that is, $k = nV_o/V_i$. When $k > 1$, this operating condition is defined as the voltage increase mode (namely, boost mode); when $k < 1$, it is defined as the voltage decrease mode (namely, buck mode); and when $k = 1$, it is defined as the matching mode. From the symmetry of the structure, it can be seen that forward/matching is equivalent to reverse/matching; forward/buck is equivalent to reverse/boost; and forward/boost is equivalent to reverse/buck. It is sufficient to study only one of the two equivalent operating conditions. In this paper, the forward and reverse buck conditions ($k < 1$) are taken as the main research objects.

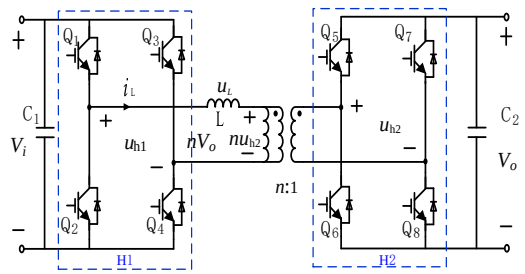


Figure 2. Topology of DAB converter.

2.1. DAB Topology and Operating Principle

The topology of the DAB converter is shown in Figure 2, which is mainly composed of two H-bridge modules, a dual-winding high-frequency transformer, and an auxiliary inductor containing the leakage inductance of the high-frequency transformer. The input and output ports of the H-bridge each have a capacitor C, V_i and V_o are the DC voltage at both ends of the converter, u_{h1} and u_{h2} are the AC side voltage of the H_1 bridge and the H_2 bridge, and u_L and i_L are the inductor voltage and current, respectively. The output port AC voltage u_{h2} is converted to the primary side u_{h2}* through the intermediate high-frequency transformer, that is, $u_{h2}^* = nu_{h2}$.

In Figure 3, D_{y1} and D_{y2} represent the duty cycles of the high levels in half a cycle for the two H-bridges, respectively, while D_a represents the duty cycle of the angle between the rising edges of the square waves of the two H-bridges in half a cycle. The DAB achieves bidirectional power transfer and efficiency optimization by changing these three variables.

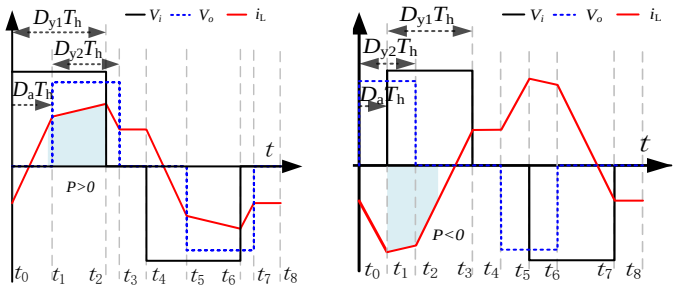


Figure 3. DAB waveform diagrams of forward and reverse transmission. (**a**) Forward transmission. (**b**) Reverse transmission.

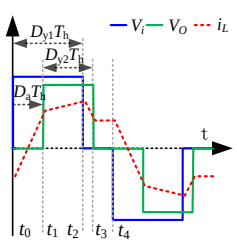
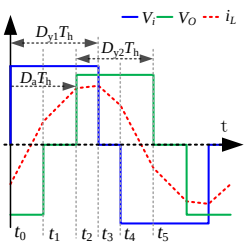
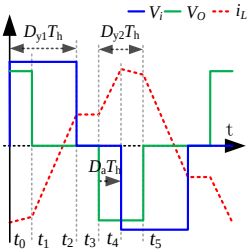
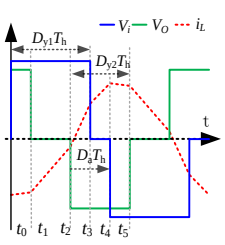
2.2. Classification of DAB Operating Modes

According to the different combinations of D_{y1}, D_{y2}, and D_a in the TPS control of the DAB, the working modes can be divided into 12 categories. According to whether D_a is greater than zero, the 12 working modes can be divided into two categories, as shown in Tables 1 and 2 [15,19]. $D_a > 0$ is mode 1.1~1.6, and $D_a < 0$ is mode 2.1~2.6. In Table 2, T_h is half of the switching period T, and both the transmission power and current are in the per-unit value, where the power reference value is $P_{base} = V_i^2/(4f_sL)$, and the current reference value is $I_{base} = V_i/(4f_sL)$. Unless otherwise specified in the figures and tables below, all power and current values are expressed in per-unit terms. The types of modes corresponding to the 3rd and 4th operating conditions (buck mode) of the DAB are shown in Table 1, where modes 1.2, 1.6, 2.4, and 2.6 are bidirectional power transfer modes [15,19]. The 5th and 6th operating conditions (boost mode) are similar to the buck mode.

Table 1. Working mode of forward and reverse power transmission under DAB bucking condition [19].

Forward/buck	**mode:** 1.1, 1.2, 1.3, 1.4, 1.5, 1.6, 2.4, 2.6
Reverse/buck	**mode:** 2.1, 2.2, 2.3, 2.4, 2.5, 2.6, 1.2, 1.6

Table 2. Characteristics of working modes of DAB converter [15,19].

$k < 1$	Mode 1.1	Mode 1.4	Mode 2.1	Mode 2.3
Waveform				
Switching Time	$t_1 = t_0 + D_a T_h$ $t_2 = t_0 + D_{y1} T_h$ $t_3 = t_0 + (D_a + D_{y2}) T_h$ $t_4 = t_0 + T_h$	$t_1 = t_0 + (D_a + D_{y2} - 1) T_h$ $t_2 = t_0 + D_a T_h$ $t_3 = t_0 + D_{y1} T_h$ $t_4 = t_0 + T_h$	$t_1 = t_0 + (D_a + D_{y2}) T_h$ $t_2 = t_0 + D_{y1} T_h$ $t_3 = t_0 + (D_a + 1) T_h$ $t_4 = t_0 + T_h$	$t_1 = t_0 + (D_a + D_{y2}) T_h$ $t_2 = t_0 + (D_a + 1) T_h$ $t_3 = t_0 + D_{y1} T_h$ $t_4 = t_0 + T_h$
Operational Constraints	$0 \le D_a \le D_{y1}$ $D_{y1} \le D_a + D_{y2} \le 1$	$0 \le D_a \le D_{y1}$ $1 \le D_a + D_{y2} \le 1 + D_{y1}$	$-(1 - D_{y1}) \le D_a \le 0$ $0 \le D_a + D_{y2} \le D_{y1}$	$-1 \le D_a \le -(1 - D_{y1})$ $0 \le D_a + D_{y2} \le D_{y1}$
Power Transfer	$-k(D_a{}^2 - 2D_aD_{y1} + D_{y1}{}^2 - D_{y2}D_{y1})$	$-k(2D_a{}^2 - 2D_aD_{y1} + 2D_aD_{y2} - 2D_a$ $+D_{y1}{}^2 - D_{y1}D_{y2} + D_{y2}{}^2 - 2D_{y2} + 1)$	$k(D_a{}^2 + 2D_aD_{y2} + D_{y2}{}^2 - D_{y1}\,D_{y2})$	$k(2D_a{}^2 - 2D_aD_{y1} + 2D_aD_{y2} + 2D_a$ $+D_{y1}{}^2 - D_{y1}\,D_{y2} - 2D_{y1} + D_{y2}{}^2 + 1)$
Power Range	$0 \sim k/3$	$0 \sim 0.5k$	$-k/3 \sim 0$	$-0.5k \sim 0$

2.3. Main Parameters

(1) Current stress

Taking mode 1.4 as an example, the inductance current function of each section in half a cycle is expressed as follows:

$$\begin{cases} I_0 = i_L(t_0) = -\frac{V_i}{4f_sL}(D_{y1} - 2k + 2kD_a + kD_{y2}) & t = t_0 \\ i_{L1}(t) = \frac{(1+k)V_i}{L}(t - t_0) - \frac{V_i}{4f_sL}(D_{y1} + kD_{y2} + 2kD_a - 2k) & t_0 < t < t_0 + (D_a + D_{y2} - 1)\frac{T_s}{2} \\ I_1 = i_L(t_1) = \frac{V_i}{4f_sL}(2D_a - D_{y1} + 2D_{y2} + kD_{y2} - 2) & t = t_0 + (D_a + D_{y2} - 1)\frac{T_s}{2} \\ i_{L2}(t) = \frac{V_i}{L}(t - t_1) + \frac{V_i}{4f_sL}[2D_a - D_{y1} + (2+k)D_{y2} - 2] & t_0 + (D_a + D_{y2} - 1)\frac{T_s}{2} < t < t_0 + D_a\frac{T_s}{2} \\ I_2 = i_L(t_2) = \frac{V_i}{4f_sL}(2D_a - D_{y1} + kD_{y2}) & t = t_0 + D_a\frac{T_s}{2} \\ i_{L3}(t) = \frac{(1-k)V_i}{L}(t - t_2) + \frac{V_i}{4f_sL}(kD_{y2} - D_{y1} + 2D_a) & t_0 + D_a\frac{T_s}{2} < t < t_0 + D_{y1}\frac{T_s}{2} \\ I_3 = i_L(t_3) = \frac{V_i}{4f_sL}(D_{y1} + 2kD_a - 2kD_{y1} + kD_{y2}) & t = t_0 + D_{y1}\frac{T_s}{2} \\ i_{L4}(t) = -\frac{kV_i}{L}(t - t_3) + \frac{V_i}{4f_sL}[(1 - 2k)D_{y1} + kD_{y2} + 2kD_a] & t_0 + D_{y1}\frac{T_s}{2} < t < t_0 + \frac{T_s}{2} \\ I_4 = i_L(t_4) = \frac{V_i}{4f_sL}(D_{y1} - 2k + 2kD_a + kD_{y2}) & t = t_0 + \frac{T_s}{2} \end{cases} \quad (1)$$

The current stress of mode 1.4 is as follows:

$$I_{L_max} = \max\{|I_0|, |I_1|, |I_2|, |I_3|\} \quad (2)$$

(2) Function expression of current RMS value and power

The RMS value formula of the inductor current in the mode 1.4 is as follows:

$$I_{L_rms} = \sqrt{\frac{2}{T_s}\left[\int_{t_0}^{t_1} i_{l1}{}^2(t)dt + \int_{t_1}^{t_2} i_{l2}{}^2(t)dt + \int_{t_2}^{t_3} i_{l3}{}^2(t)dt + \int_{t_3}^{t_4} i_{l4}{}^2(t)dt\right]} \quad (3)$$

The formula of the average value of the inductor current in the mode 1.4 is as follows:

$$\begin{aligned} I_{L_avg} &= \frac{2}{T_s}\left[\int_{t_0}^{t_1} i_{l1}(t)dt + \int_{t_1}^{t_2} i_{l2}(t)dt + \int_{t_2}^{t_3} i_{l3}(t)dt + \int_{t_3}^{t_4} i_{l4}(t)dt\right] \\ &= -\frac{kV_i}{4f_sL}(2D_a{}^2 - 2D_aD_{y1} + 2D_aD_{y2} - 2D_a + D_{y1}{}^2 - D_{y1}D_{y2} + D_{y2}{}^2 - 2D_{y2} + 1) \end{aligned} \quad (4)$$

Its output power is as follows:

$$P = V_i I_{L_avg} = -\frac{kV_i{}^2}{4f_sL}(2D_a{}^2 - 2D_aD_{y1} + 2D_aD_{y2} - 2D_a + D_{y1}{}^2 - D_{y1}D_{y2} + D_{y2}{}^2 - 2D_{y2} + 1) \quad (5)$$

3. Double-Objective Optimization Process

In order to better explore the inherent regularities of each working mode, the optimization results of stress optimization, RMS optimization, and dual-objective entropy weight method optimization will be analyzed and compared. According to [10,19], the 12 modes can be equivalently simplified into four locally optimal modes. This paper conducts optimization research based on these four locally optimal modes.

3.1. Selection of Optimization Objectives

In this paper, when performing double-objective genetic algorithm optimization for current stress and RMS values, a set of Pareto solutions is first obtained, and then the relatively optimal solution is selected from this set. When there is only one solution in the Pareto solution set, it shows that the minimum stress and the minimum RMS are the same point; when there are multiple solutions in the Pareto solution set, it shows that the minimum of the two is not the same point. In the case that the minimums of the two objectives are not at the same point, it is usually necessary to set a certain weight for multiple objectives to determine the optimal solution. Three weights are set in this paper: when the weights of the two objectives are set to 0:1 and 1:0 respectively, which is equivalent to two single-objective optimizations, it can be regarded as single-objective optimization of the current stress and single-objective optimization of the RMS value (referred to as stress optimization and RMS optimization). Considering that these weights only consider a single target, the third weight adopts the technique for order preference by similarity to ideal solution (TOPSIS) with entropy weight to screen out the relatively optimal solution. The entropy weight method is an objective weighting method that calculates the entropy weight of each indicator based on its degree of variation using information entropy. The entropy weights are then used to adjust the weights of each indicator, resulting in more objective indicator weights.

3.2. The Optimization Process of Three Different Optimization Objectives

In this section, a double-objective genetic algorithm is employed to simultaneously optimize both the RMS and stress to obtain a set of Pareto-optimal solutions. Subsequently, different weights are assigned to these solutions in order to obtain the optimal solutions for different optimization objectives. The three optimization variables are D_{y1}, D_{y2}, and D_a; the constraint conditions include the range constraints of each working mode, the upper and lower bound constraints of the variables, and transmission power constraints. As shown in Table 3, there are three different target optimization processes in working mode 1.4, and the optimization processes of other modes are similar to those of mode 1.4. The RMS and stress of the other modes are shown in Appendix A, Tables A3 and A4.

Table 3. Genetic optimization with three different optimization objectives (mode 1.4).

Optimization Method	Double-Objective Genetic Algorithm		
	Weight Ratio 1:0 RMS Single-Objective Optimization	**Weight Ratio 0:1 Stress Single-Objective Optimization**	**Double-Objective Entropy Weight Method Optimization**
Objective function	$\min\{I_{L_rms}, I_{L_\max}\}$		
Linear constraint	Operating mode range constraint: $0 \le D_a \le D_{y1}, D_{y1} \le D_a + D_{y2} \le 1$		
	Variable upper and lower bound constraints: $0 \le D_{y1} \le 1, 0 \le D_a \le 1, 0 \le D_{y2} \le 1, 0 \le k \le 1$		
Nonlinear constraint	Transmission power constraint: $P = -\frac{V_i^2}{4f_sL}k({D_a}^2 - 2D_aD_{y1} + {D_{y1}}^2 - D_{y2}D_{y1})$		

Therein, we have the following:

$$\begin{cases} I_{L_rms} = \sqrt{\frac{2}{T_s}\left[\int_{t_0}^{t_1} {i_{L1}}^2(t)dt + \int_{t_1}^{t_2} {i_{L2}}^2(t)dt + \int_{t_2}^{t_3} {i_{L3}}^2(t)dt + \int_{t_3}^{t_4} {i_{L4}}^2(t)dt\right]} \\ I_{L_\max} = \max\{|I_0|, |I_1|, |I_2|, |I_3|\} \end{cases}$$

4. Analysis of Optimal Control Variables in Local Optimal Mode

According to the voltage matching characteristics between the two ports, this section conducts an in-depth study on the buck operating condition (k < 1) under voltage mismatch. Building on the analysis of the optimization results of three different optimizations for the four locally optimal modes, this section summarizes the regularities between the optimization variables of each locally optimal mode in different power segments, considering the two parameters of k and P. Based on these regularities, the function expression of the relevant optimal control variables is derived.

4.1. Optimal Control Variables for Different Power Ranges in Mode 1.4

According to [5,19], the regularities between the optimization variables of different power segments in different local optimal modes do not change with the value of k, meaning that the corresponding regularities between the optimization variables remain fixed for any value of k within the range [0, 1]. In this section, using the optimization algorithm from the previous section, we obtained the variation charts of the optimization variables for the three optimizations in the full-power range when k was set to 0.8, as shown in Figure 4.

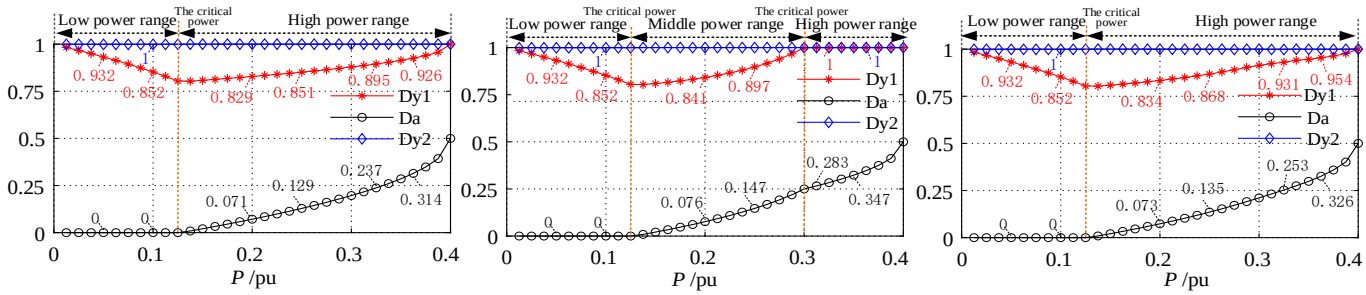


Figure 4. The optimization variables of working mode 1.4 in full-power range when k = 0.8. (**a**) Stress single-objective optimization. (**b**) RMS single-objective optimization. (**c**) Double-objective entropy weight method optimization.

Upon analyzing and comparing the optimization results of the three optimizations in Figure 4, we found the regularities between the optimization variables in the different power segments for the three optimizations: the three optimizations have the same regularities in the low-power segment, that is, D_{y2} = 1, and D_a = 0; the stress optimization and the double-objective entropy weight method optimization have the same rules in the high-power section, that is, D_{y2} = 1; the RMS optimization exists in the middle-power section and the high-power section, and the regularities are D_{y2} = 1 and D_{y1} = D_{y2} = 1, respectively, as shown in Tables 4 and 5.

Table 4. The rule of control variables in different power segments under stress optimization and double-objective entropy weight method optimization of mode 1.4.

Power Range	Low-Power Range	Critical Power	High-Power Range
Regularities of Optimization variables	$\begin{cases} D_a = 0 \\ D_{y2} = 1 \end{cases}$	$\begin{cases} D_{y2} = k \\ D_a = 0 \\ D_{y2} = 1 \end{cases}$	$D_{y2} = 1$

Table 5. The rule of the RMS optimization variables in different power segments of mode 1.4.

Power Range	Low-Power Range	Critical Power	Middle-Power Range	Critical Power	High-Power Range
Regularities of optimization variables	$\begin{cases} D_a = 0 \\ D_{y2} = 1 \end{cases}$	$\begin{cases} D_{y2} = k \\ D_a = 0 \\ D_{y2} = 1 \end{cases}$	$D_{y2} = 1$	$\begin{cases} D_{y1} = 1 \\ D_{y2} = 1 \end{cases}$	$\begin{cases} D_{y1} = 1 \\ D_{y2} = 1 \end{cases}$

4.1.1. Calculation Methods for Optimized Control Variables Under Three Optimization Approaches in the Low-Power Range

Figure 4 compares the results of the three optimization variables in the low-power range: the optimization results of stress optimization, RMS optimization, and double-objective entropy weight method optimization are all at the same point, that is, the minimum stress and minimum RMS value were achieved at the same point.

Substituting the regularities for the low-power range from Tables 4 and 5, specifically, $D_{y2} = 1$ and $D_a = 0$, into the power transmission expression for mode 1.4 in Table 2,

$$P = -k(2{D_a}^2 - 2D_aD_{y1} + 2D_aD_{y2} - 2D_a + {D_{y1}}^2 - D_{y1}D_{y2} + {D_{y2}}^2 - 2D_{y2} + 1) \quad (6)$$

we obtain

$$D_{y1} = \frac{1}{2} \pm \sqrt{\frac{1}{4} - \frac{P}{k}},\ D_a = 0,\ D_{y2} = 1 \quad (7)$$

By substituting the optimized control variables in (7) into the expression for the stress function of mode 1.4, the expression for the minimum stress can be deduced:

$$\min I_3 = D_{y1} + 2kD_a - 2kD_{y1} + kD_{y2} = (1 - 2k)D_{y1} + k = \frac{1}{2} \pm (1 - 2k)\sqrt{\frac{1}{4} - \frac{P}{k}} \quad (8)$$

By substituting the optimized control variables in (7) into the expression for the RMS value function of mode 1.4 to obtain the expression for the minimum RMS value, we have the following:

$$I_{rms_\min} = \sqrt{\pm(\frac{1}{2} - k)(\frac{2}{3} + \frac{4}{3}\frac{P}{k})\sqrt{\frac{1}{4} - \frac{P}{k}} + \frac{1}{3}k^2 - \frac{1}{3}k + \frac{1}{6}} \quad (9)$$

According to the value range of k, it can be deduced that

$$\begin{aligned} &When\ k \le\ 0.5,\ D_{y1} = \tfrac{1}{2} - \sqrt{\tfrac{1}{4} - \tfrac{P}{k}},\ D_a = 0,\ D_{y2} = 1, \\ &\min I_3 = \tfrac{1}{2} - (1 - 2k)\sqrt{\tfrac{1}{4} - \tfrac{P}{k}} \quad I_{rms_\min} = \sqrt{-(\tfrac{1}{2} - k)(\tfrac{2}{3} + \tfrac{4}{3}\tfrac{P}{k})\sqrt{\tfrac{1}{4} - \tfrac{P}{k}} + \tfrac{1}{3}k^2 - \tfrac{1}{3}k + \tfrac{1}{6}} \end{aligned} \quad (10)$$

$$\begin{aligned} &When\ k > 0.5,\ D_{y1} = \tfrac{1}{2} + \sqrt{\tfrac{1}{4} - \tfrac{P}{k}},\ D_a = 0,\ D_{y2} = 1, \\ &\min I_3 = \tfrac{1}{2} + (1 - 2k)\sqrt{\tfrac{1}{4} - \tfrac{P}{k}} \quad I_{rms_\min} = \sqrt{(\tfrac{1}{2} - k)(\tfrac{2}{3} + \tfrac{4}{3}\tfrac{P}{k})\sqrt{\tfrac{1}{4} - \tfrac{P}{k}} + \tfrac{1}{3}k^2 - \tfrac{1}{3}k + \tfrac{1}{6}} \end{aligned} \quad (11)$$

4.1.2. Calculation Methods for Optimized Control Variables Under Two Optimizations in the Medium- and High-Power Ranges

From the comparison of the three optimization variable results in the medium- and high-power segments shown in Figure 4, it is evident that the optimization results for current stress optimization, RMS optimization, and double-objective entropy weight method optimization are not at the same point. However, the optimization results of these three points are very close. Based on these rules, the stress optimization control variables and the RMS value optimization control variables were derived by using the trigonometric function polar coordinate method.

(1) Calculation Method for Control Variables in High-Power Range Under Stress Optimization

The regularity for the high-power range in Table 4 is given by

$$D_{y2} = 1 \tag{12}$$

By substituting (12) into the power transfer expression (6) for mode 1.4, we obtain

$$P = k(-2{D_a}^2 + 2D_a D_{y1} - {D_{y1}}^2 + D_{y1}) \tag{13}$$

Further simplification yields the following:

$$1 - \frac{2P}{k} = (2D_a - D_{y1})^2 + (D_{y1} - 1)^2 \tag{14}$$

Let

$$b^2 = 1 - \frac{2P}{k} \tag{15}$$

$$\begin{aligned} &b^2 = (2D_a - D_{y1})^2 + (D_{y1} - 1)^2 \\ &D_{y1} = 1 - b\cos\theta,\ D_a = \tfrac{1}{2}(1 - b\cos\theta - b\sin\theta) \end{aligned} \tag{16}$$

In (16), b and θ are intermediate variables. By substituting (12) and (16) into the expression for the stress function, we obtain the following:

$$\min I_3 = D_{y1} + 2kD_a - 2kD_{y1} + kD_{y2} = (1 - 2k)D_{y1} + kD_a + k \tag{17}$$

$$\begin{aligned} \min I_3 &= 1 - b[(1-k)\cos\theta + k\sin\theta] = 1 - b\sqrt{(1-k)^2 + k^2}\sin(\theta + \alpha) \\ &= 1 - b\sqrt{(1-k)^2 + k^2} = 1 - \sqrt{1 - \tfrac{2P}{k}}\sqrt{(1-k)^2 + k^2} \end{aligned} \tag{18}$$

$$Of\ which\ : \sin(\theta + \alpha) = 1 \quad I_3 \min\ \sin\theta = \cos\alpha = \frac{k}{\sqrt{k^2 + (1-k)^2}} \quad \cos\theta = \sin\alpha = \frac{(1-k)}{\sqrt{k^2 + (1-k)^2}} \tag{19}$$

In (19), b, a and θ are intermediate variables. By substituting (15) and (19) into (16) and (17), we derive the following:

$$\min I_3 = 1 - \sqrt{1 - \frac{2P}{k}}\sqrt{(1-k)^2 + k^2} \quad D_{y1} = 1 - (1-k)\frac{\sqrt{1 - \frac{2P}{k}}}{\sqrt{(1-k)^2 + k^2}} \quad D_a = \frac{1}{2} - \frac{1}{2}\frac{\sqrt{1 - \frac{2P}{k}}}{\sqrt{(1-k)^2 + k^2}},\ D_{y2} = 1 \tag{20}$$

(2) Calculation Method for Control Variables in the Medium- and High-Power Ranges Under RMS Optimization

(a) Calculation Method for Control Variables in the Medium-Power Range Under RMS Optimization

The expression for the squared RMS value of the current in mode 1.4 is as follows:

$$\begin{aligned} I_{rms}^2 = &-\tfrac{8}{3}kD_a^3 + 4kD_a^2 D_{y1} - 4kD_a^2 D_{y2} + 4kD_a^2 - 4kD_a D_{y1}^2 + 4kD_a D_{y1} D_{y2} - 4kD_a D_{y2}^2 + 8kD_a D_{y2} - 4kD_a + \\ &\tfrac{4}{3}kD_{y1}^3 - \tfrac{2}{3}D_{y1}^3 - 2kD_{y1}^2 D_{y2} + D_{y1}^2 + 2kD_{y1}D_{y2}^2 - 2kD_{y1}D_{y2} - \tfrac{2}{3}k^2 D_{y2}^3 - \tfrac{4}{3}kD_{y2}^3 + k^2 D_{y2}^2 + 4kD_{y2}^2 - 4kD_{y2} + \tfrac{4}{3}k \end{aligned} \tag{21}$$

By substituting the rule of the medium-power section in Table 4, $D_{y2} = 1$ into (21), we derive the following:

$$I_{rms}^2 = -\frac{8}{3}kD_a^3 + 4kD_a^2 D_{y1} - 4kD_a D_{y1}^2 + 4kD_a D_{y1} + \frac{4}{3}kD_{y1}^3 - \frac{2}{3}D_{y1}^3 - 2kD_{y1}^2 + D_{y1}^2 + \frac{1}{3}k^2 \tag{22}$$

Substituting $D_{y1} = 1 - b\cos\theta$, $D_a = \frac{1}{2}(1 - b\cos\theta - b\sin\theta)$ in (16) into (22), we obtain the following:

$$I_{rms}^2 = f(k, b, \theta)$$

To find the minimum of the RMS value squared, set $\partial I_{rms}^2/\partial\theta = 0$ to obtain the minimum point:

$$\frac{\partial I_{rms}^2}{\partial\theta} = \frac{1}{3}bcos\theta\Big[(2kcos^2\theta - 6cos\theta sin\theta - 4ksin^2\theta + k)b^2 + 6bsin\theta - 3k\Big] = 0 \Rightarrow \theta \quad (23)$$

It can be obtained from the above equation that θ may have multiple extreme points. In order to prove that the extreme point is the minimum point, it is necessary to judge whether $\partial^2(I_{rms}^2)/\partial\theta^2$ is greater than 0.

$$\frac{\partial^2(I_{rms}^2)}{\partial\theta^2} = \Big[(-6cos^3\theta - 6ksin\theta cos^2\theta + 4cos\theta + ksin\theta)b^3 + (4cos^2\theta - 2)b^2 + kbsin\theta\Big] \quad (24)$$

When the extreme point θ is substituted into (24), there may be multiple cases that satisfy $\partial I_{rms}^2/\partial\theta > 0$. It is necessary to first substitute multiple extreme points θ into the polar coordinates of the trigonometric function to obtain D_{y1}, D_{y2}, and D_a, and then it is necessary to judge whether these three variables meet the mode range. Subsequently, select those that meet the conditions, and then compare the corresponding extreme points, select the extreme point corresponding to the minimum value, and take this extreme point as the minimum point; finally, the control variable corresponding to the selected minimum point θ is selected as the optimized control variable for RMS value minimization.

(b) Calculation Method for Control Variables in the High-Power Range Under RMS Optimization

By substituting the rule of the high-power section in Table 4, $D_{y1} = D_{y2} = 1$, into the power transmission expression (6) of mode 1.4, we derive the following:

$$D_{y1} = 1, D_{y2} = 1, D_a = \frac{1 - \sqrt{1 - 2P}}{2} \quad (25)$$

By substituting the optimized control variable (25) into the RMS value function expression (21) of mode 1.4, the minimum RMS value expression is obtained as follows:

$$I_{rms_\min} = \sqrt{-\frac{2}{3}k(1 - 2P)^{\frac{1}{2}}(1 + P) + \frac{1}{3}k^2 + \frac{1}{3}} \quad (26)$$

4.1.3. Calculation Method for Optimized Control Variables at the Common Power Boundary Point Under Both Stress Optimization and RMS Optimization

The boundary point between the low- and high-power segments in stress optimization and the boundary point between the low and medium power segments in RMS optimization are the same point, which is referred to as the critical power point. The critical rule for the critical power point is obtained from Table 4:

$$D_{y1} = k, D_{y2} = 1, D_a = 0 \quad (27)$$

By substituting (27) into the power transmission expression (6) of mode 1.4 in Table 2, the critical power is defined as follows:

$$P = k^2(1 - k) \quad (28)$$

By substituting the optimized control variable (27) into the stress function expression of mode 1.4, this results in the minimum stress expression, which is denoted as follows:

$$\min I_3 = D_{y1} + 2kD_a - 2kD_{y1} + kD_{y2} = 2k(1 - k) \quad (29)$$

By substituting the optimization control variable (27) into the RMS value function expression (21) of model 1.4 to obtain the expression of the minimum RMS value, we obtain the following equation:

$$I_{rms_\min} = \frac{2\sqrt{3}}{3}k(1-k) \tag{30}$$

4.1.4. Calculation Method for Optimized Control Variables at the Boundary Point Between Medium- and High-Power Ranges Under RMS Optimization

The boundary between the medium- and high-power segments is $D_{y1} = 1$. We substitute this into the trigonometric function polar coordinate (16) $D_{y1} = 1 - b\cos\theta$ to obtain $\cos\theta = 0$.

We substitute $\cos\theta = 0$ into (24) to obtain $\frac{\partial I_{rms}^2}{\partial\theta} = 0$. From the above analysis, it is concluded that $\cos\theta = 0 \Rightarrow \theta = 2k\pi + \frac{\pi}{2}$ or $\theta = 2k\pi + \frac{3\pi}{2}, (k = 1, 2\ldots)$ is the extreme point of I_{rms}^2.

To confirm that the extreme point is a minimum point, it needs to satisfy the condition $\frac{\partial^2(I_{rms}^2)}{\partial\theta^2} > 0$. When $\theta = 2k\pi + \frac{3}{2}\pi$, $\frac{\partial^2(I_{rms}^2)}{\partial\theta^2} > 0$ is not satisfied, so it is discarded. Substituting $\theta = 2k\pi + \frac{\pi}{2}$ into $\frac{\partial^2(I_{rms}^2)}{\partial\theta^2}$ in (24) yields the following:

$$\begin{aligned}\frac{\partial^2(I_{rms}^2)}{\partial\theta^2} &= ksin\theta b^3 - 2b^2 + kbsin\theta = b(kb^2 - 2b + k)\\ &= b\left[k(1-\tfrac{2P}{k}) - 2\sqrt{1-\tfrac{2P}{k}} + k\right] = 2\sqrt{1-\tfrac{2P}{k}}\left[k - P - \sqrt{1-\tfrac{2P}{k}}\right] > 0\end{aligned} \tag{31}$$

Then,

$$\left[k - P - \sqrt{1-\frac{2P}{k}}\right] > 0 \tag{32}$$

should be satisfied so that

$$k - P - \sqrt{1-\frac{2P}{k}} = 0 \Rightarrow k^3 - 2k^2P + (P^2-1)k + 2P = 0 \Rightarrow P_{linjie1.4} \tag{33}$$

The critical point between the middle- and high-power segments, the critical rule, is defined as follows:

$$D_{y1} = 1, D_{y2} = 1, D_a = \frac{1-\sqrt{1-2P}}{2} \tag{34}$$

By substituting the optimized control variable (34) into the RMS value function expression (21) for mode 1.4, the minimum RMS value expression is deduced as follows:

$$I_{rms_\min} = \sqrt{-\frac{2}{3}k(1-2P)^{\frac{1}{2}}(1+P) + \frac{1}{3}k^2 + \frac{1}{3}} \tag{35}$$

Based on the expressions of the stress-optimal control variables and the minimum stresses of (10), (11), and (20) in the low- and high-power segments of mode 1.4, as well as the related expressions (27)–(30) for the boundary points, the expressions of the stress optimal control variables and the minimum stress in the full power range were comprehensively obtained, as shown in Table 6.

According to the expressions of the RMS optimal control variables and the minimum RMS values of (10), (11), and (23)–(26) in the low-, medium- and high-power segments of mode 1.4, as well as the related expressions of (27)–(30) and (33)–(35) for the low-to-medium and medium-to-high boundary points, the expressions of the RMS optimal control variables and the minimum RMS value in the full-power range were comprehensively obtained, as shown in Table 7.

Table 6. The stress variable regularity and stress optimal control variables of DAB in different power sections in the full-power range of mode 1.4.

$k < 1$	Power Range	Variable Regularity	Stress Optimal Control Parameters and the Minimum Stress Value
Mode 1.4 $p > 0$	Low-power range $0 < P < k^2(1-k)$	$\begin{cases} D_a = 0 \\ D_{y2} = 1 \end{cases}$	$k \le 0.5 : D_{y1} = \frac{1}{2} - \sqrt{\frac{1}{4} - \frac{P}{k}},\ D_a = 0,\ D_{y2} = 1,\ \min I_3 = \frac{1}{2} - (1-2k)\sqrt{\frac{1}{4} - \frac{P}{k}}$
			$k > 0.5 : D_{y1} = \frac{1}{2} + \sqrt{\frac{1}{4} - \frac{P}{k}},\ D_a = 0,\ D_{y2} = 1,\ \min I_3 = \frac{1}{2} + (1-2k)\sqrt{\frac{1}{4} - \frac{P}{k}}$
	Critical power $P = k^2(1-k)$		$D_{y1} = k, D_a = 0, D_{y2} = 1,\ \min I_2 = 2k(1-k)$
	High-power range $k^2(1-k) < P < k/2$	$D_{y2} = 1$	$D_{y1} = 1 - (1-k)\frac{\sqrt{1-\frac{2P}{k}}}{\sqrt{(1-k)^2+k^2}},\ D_a = \frac{1}{2} - \frac{1}{2}\frac{\sqrt{1-\frac{2P}{k}}}{\sqrt{(1-k)^2+k^2}},\ D_{y2} = 1, \min I_3 = 1 - \sqrt{1-\frac{2P}{k}}\sqrt{(1-k)^2+k^2}$

Table 7. The RMS variable regularity and RMS optimal control variables of DAB in different power sections in the full-power range of mode 1.4.

$k < 1$	Power Range	Variable Regularity	RMS Optimal Control Parameters and the Minimum RMS Value
Mode 1.4 $p > 0$	Low-power range $0 < P < k^2(1-k)$	$\begin{cases} D_a = 0 \\ D_{y2} = 1 \end{cases}$	$k \le 0.5 : D_{y1} = \frac{1}{2} - \sqrt{\frac{1}{4} - \frac{P}{k}},\ D_a = 0, D_{y2} = 1\ \ I_{rms_\min} = \sqrt{-(\frac{1}{2}-k)(\frac{2}{3} + \frac{4}{3}\frac{P}{k})\sqrt{0.25 - \frac{P}{k}} + \frac{1}{3}k^2 - \frac{1}{3}k + \frac{1}{6}}$
			$k > 0.5 : D_{y1} = \frac{1}{2} + \sqrt{\frac{1}{4} - \frac{P}{k}},\ D_a = 0, D_{y2} = 1\ \ I_{rms_\min} = \sqrt{(\frac{1}{2}-k)(\frac{2}{3} + \frac{4}{3}\frac{P}{k})\sqrt{0.25 - \frac{P}{k}} + \frac{1}{3}k^2 - \frac{1}{3}k + \frac{1}{6}}$
	Critical power $P = k^2(1-k)$	$\begin{cases} D_{y1} = k \\ D_a = 0 \\ D_{y2} = 1 \end{cases}$	$D_{y1} = k, D_a = 0, D_{y2} = 1\ \ I_{rms_\min} = \frac{2\sqrt{3}}{3}k(1-k)$
	Middle-power range $k^2(1-k) < P < P_{linjie1.4}$	$D_{y2} = 1$	$\frac{\partial I_{rms}^2}{\partial \theta} = (2kcos^2\theta - 6cos\theta sin\theta - 4ksin^2\theta + k)b^2 + 6bsin\theta - 3k = 0 \Rightarrow \theta$ θ may have multiple solutions, and the unique solution of θ is determined based on the minimum value constraint condition, wherein it is substituted into the trigonometric function in the polar coordinates. $let: b^2 = 1 - \frac{2P}{k},\ b^2 = (2D_a - D_{y1})^2 + (D_{y1} - 1)^2 \Rightarrow D_{y1} = 1 - b\cos\theta,\ D_{y2} = 1,\ D_a = \frac{1}{2}(1 - b\cos\theta - b\sin\theta)$. $I_{rms}^2 = -\frac{8}{3}kD_a^3 + 4kD_a^2D_{y1} - 4kD_aD_{y1}^2 + 4kD_aD_{y1} + \frac{4}{3}kD_{y1}^3 - \frac{2}{3}D_{y1}^3 - 2kD_{y1}^2 + D_{y1}^2 + \frac{1}{3}k^2$.
	Critical power $P_{linjie1.4}$		$D_{y1} = 1, D_{y2} = 1, D_a = \frac{1-\sqrt{1-2P}}{2}\ \ I_{rms_\min} = \sqrt{-\frac{2}{3}k(1-2P)^{\frac{1}{2}}(1+P) + \frac{1}{3}k^2 + \frac{1}{3}}$ $k - P - \sqrt{1 - \frac{2P}{k}} = 0 \Rightarrow k^3 - 2k^2P + (P^2 - 1)k + 2P = 0 \Rightarrow P_{linjie1.4}$
	High-power range $P_{linjie1.4} < P < k/2$	$\begin{cases} D_{y1} = 1 \\ D_{y2} = 1 \end{cases}$	$D_{y1} = 1, D_{y2} = 1, D_a = \frac{1-\sqrt{1-2P}}{2}\ \ I_{rms_\min} = \sqrt{-\frac{2}{3}k(1-2P)^{\frac{1}{2}}(1+P) + \frac{1}{3}k^2 + \frac{1}{3}}$

4.2. Summary of Regularities and Derivation of Optimized Control Variables for Other Local Optimal Modes

For modes 1.1, 2.1, and 2.3, the double-objective optimization, rule summary, and the derivation method of the optimal control variables are similar to those of mode 1.4, and the derivation process is shown in Figure 5. Initially, a double-objective genetic algorithm for stress and RMS was employed to optimize the locally optimal modes and obtain the Pareto-optimal solutions in the full-power range for different k values. Subsequently, based on the set weights, the optimal solutions for the stress optimization, RMS optimization, and double-objective entropy weight method optimization were obtained, and the optimization results for the three optimizations at different k values were analyzed and compared. Next, the rules between the optimization variables for the three optimizations in different power segments were summarized, and it was found that the rules among the optimization variables for the three optimizations are the same at different k values [5,8,19]. Lastly, the rules among the optimization variables of the three different optimizations were analyzed and compared, revealing that the rules for stress optimization and dual-objective entropy weight method optimization are the same in different power segments, and the rules for all three optimizations are the same in the low-power segment.

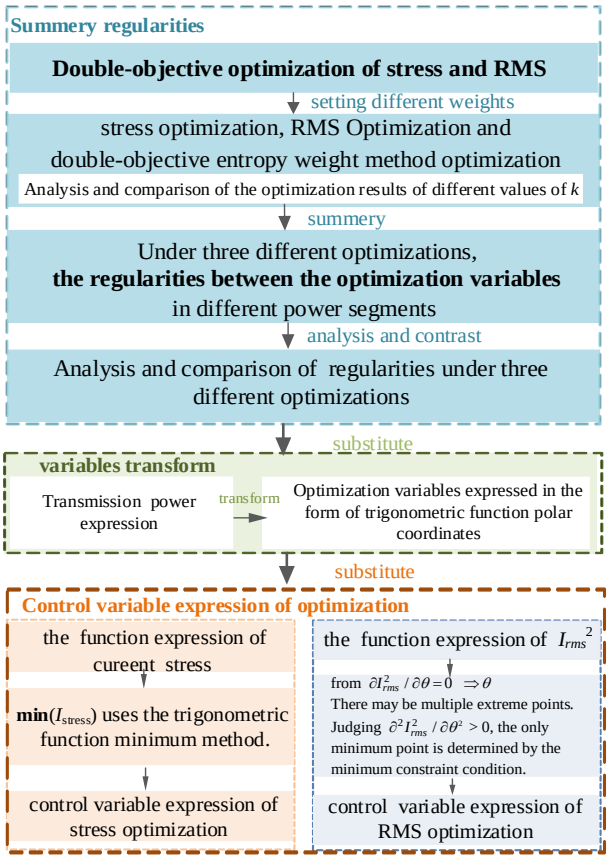


Figure 5. Derivation flow chart of stress and RMS optimization control variables.

Based on the derived rules, they were substituted into the corresponding power transmission expression (Table 2), and the optimization variables were transformed into a trigonometric function polar coordinate form, as shown in Table A2; then, these optimization variables were substituted into the stress function expression and the RMS function expression. Then, the function expression of the stress optimization control variables was derived by using the minimum value method of the trigonometric function [19]. Finally, the function expression of RMS optimization control variables was derived using the RMS value extreme point method. In Figure 5, the extreme point θ obtained from $\partial(I_{rms}^2)/\partial\theta = 0$ may have multiple solutions. To identify the unique minimum point, the following minimum point constraint conditions must be met:

(1) Satisfy $\partial^2(I_{rms}^2)/\partial\theta^2 > 0$ to ensure that the extreme point is the minimum point, where the $\partial^2(I_{rms}^2)/\partial\theta^2$ values are provided in Table A3;
(2) The values of D_{y1}, D_{y2}, and D_a derived from substituting the extreme point θ into the trigonometric polar coordinates need to satisfy the range of the working mode;
(3) The value of θ corresponding to the minimum point should be the smallest among all the values of θ corresponding to the extreme points.

By analyzing the optimization results of the three optimizations of any value of k from 0 to 1, it is concluded that the rules between the optimization variables of the three optimizations in different power segments in these four modes are the same at any value of k ($0 < k < 1$) [8,19]. Taking $k = 0.8$ as an example, according to the optimization results of the three optimizations, the variation diagrams of the optimization variables of modes 1.1, 2.1, and 2.3 in the full-power range under the three optimizations were obtained, as shown in Figures 6–8. Through the analysis and comparison of the three optimization results in Figures 6–8, we found that there are different rules between optimization variables in different power sections, as shown in Tables 8–11.

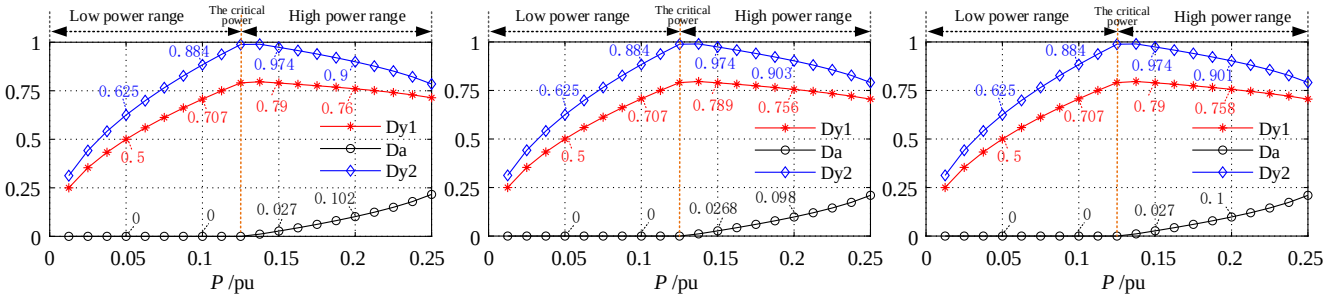


Figure 6. The optimization variables of working mode 1.1 in full-power range when $k = 0.8$. (**a**) Stress single-objective optimization. (**b**) RMS single-objective optimization. (**c**) Double-objective entropy weight method optimization.

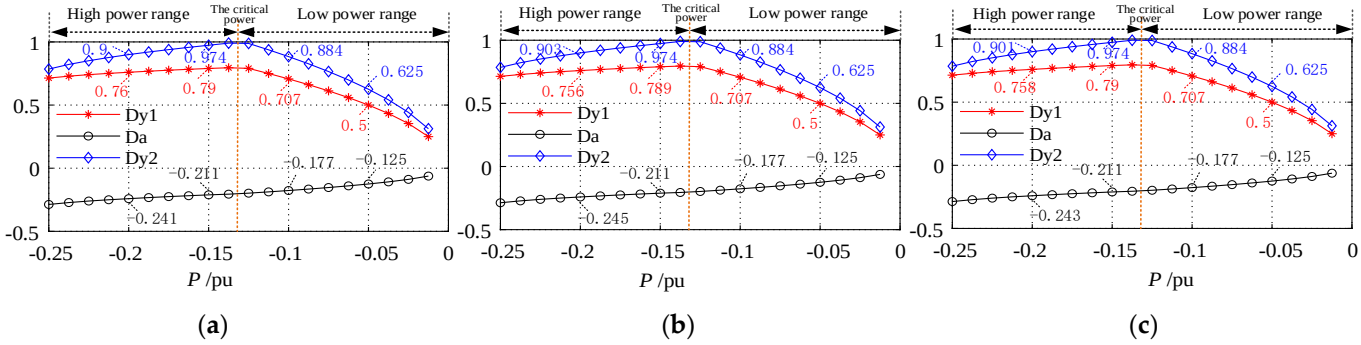


Figure 7. The optimization variables of working mode 2.1 in full power range when $k = 0.8$. (**a**) Stress single-objective optimization. (**b**) RMS single-objective optimization. (**c**) Double-objective entropy weight method optimization.

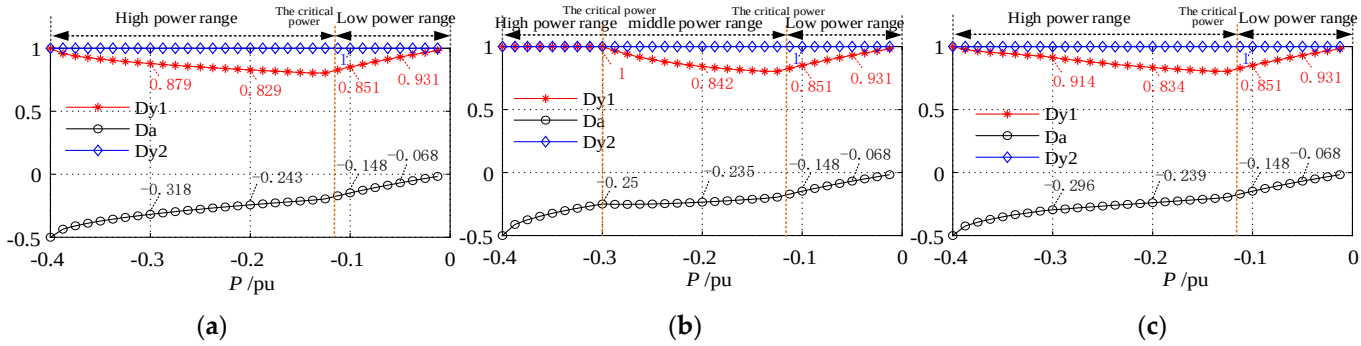


Figure 8. The optimization variables of working mode 2.3 in full power range when $k = 0.8$. (**a**) Stress single-objective optimization. (**b**) RMS single-objective optimization. (**c**) Double-objective entropy weight method optimization.

Table 8. The rule of the optimization variables of the three optimization objectives in different power segments of mode 1.1.

Power Range	Low-Power Range	Critical Power	High-Power Range
Regularities of optimization variables	$\begin{cases} D_{y1} = kD_{y2} \\ D_a = 0 \end{cases}$	$\begin{cases} D_{y1} = kD_{y2} \\ D_a = 0 \\ D_a + D_{y2} = 1 \end{cases}$	$D_a + D_{y2} = 1$

Table 9. The rule of the optimization variables of the three optimization objectives in different power segments of mode 2.1.

Power Range	Low-Power Range	Critical Power	High-Power Range
Regularities of optimization variables	$\begin{cases} D_{y1} = kD_{y2} \\ D_{y1} - D_a = D_{y2} \end{cases}$	$\begin{cases} D_{y1} = k \\ D_a = k-1 \\ D_{y2} = 1 \end{cases}$	$D_{y1} - D_a = 1$

Table 10. The rule of control variables in different power segments under stress optimization and double-objective entropy weight method optimization of mode 2.3.

Power Range	Low-Power Range	Critical Power	High-Power Range
Regularities of optimization variables	$\begin{cases} D_{y1} - D_a = 1 \\ D_{y2} = 1 \end{cases}$	$\begin{cases} D_{y1} = k \\ D_a = k-1 \\ D_{y2} = 1 \end{cases}$	$D_{y2} = 1$

Table 11. The rule of the RMS optimization variables in different power segments of mode 2.3.

Power Range	Low-Power Range	Critical Power	Middle-Power Range	Critical Power	High-Power Range
Regularities of optimization variables	$\begin{cases} D_{y1} - D_a = 1 \\ D_{y2} = 1 \end{cases}$	$\begin{cases} D_{y1} = k \\ D_a = k-1 \\ D_{y2} = 1 \end{cases}$	$D_{y2} = 1$	$\begin{cases} D_{y1} = 1 \\ D_{y2} = 1 \end{cases}$	$\begin{cases} D_{y1} = 1 \\ D_{y2} = 1 \end{cases}$

The analysis of the optimization results shows that, for modes 1.1 and 2.1, the rules in different power segments under the three optimizations are the same, and the three optimization results are identical in the entire power range, indicating that the minimum stress and RMS values were achieved at the same point. For modes 1.4 and 2.3, the rules in the low-power segment under the three optimizations are the same, and the three optimization results are identical in the low-power segment, indicating that the minimum stress and RMS values were also achieved at the same point.

For modes 1.4 and 2.3, the regularities in the high-power segment under stress optimization and dual-objective entropy weight method optimization are the same, but the optimization results of the two are different. In the RMS optimization for modes 1.4 and 2.3, a notable difference can be observed compared to the other two optimizations: a mid-power segment follows the rule of $D_{y2} = 1$, while in the high-power segment, the rule is $D_{y1} = D_{y2} = 1$. The specific derivation processes of the optimal control variables in these three modes are similar to those for mode 1.4 in the previous section. The derivation conclusions are presented in [19] and Table A1.

5. Selection of Global Optimal Mode in the Full Power Range

We found an overlap of transmission power between the local optimal modes 1.1 and 1.4 and between modes 2.1 and 2.3. In the power overlap interval, based on the expression of the minimum stress function and the expression of the minimum RMS function derived in the previous section, the global optimal control variables for the stress values, the global optimal control variables for the RMS values, and the comprehensive global optimal working mode in the full-power range were selected.

5.1. Quantitative Analysis

When conducting an optimization analysis of the full-power range of DAB, this section took $k = 0.8$ as a specific case for quantitative analysis. Figure 9 shows the optimization results with $k = 0.8$ under the three optimizations. For forward transmission, in the low-power segment (0 pu to 0.128 pu), mode 1.1 yielded lower current stress and RMS values

than mode 1.4 at the same power; in the high-power segment (0.128 pu to 0.267 pu), mode 1.4 yielded lower values. For reverse transmission, in the low-power segment (−0.128 pu to 0), mode 2.1 yielded lower current stress and RMS values than mode 2.3 at the same power; in the high-power segment (−0.128 pu to −0.267 pu), mode 2.3 yielded lower values.

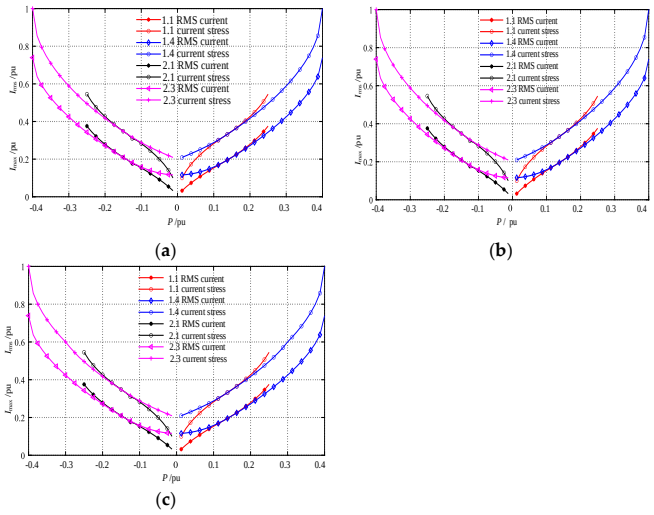


Figure 9. Three optimization results: Current RMS values and stress values of four working modes when k = 0.8. (**a**) Double-objective entropy weight method optimization. (**b**) Stress single-objective optimization. (**c**) RMS single-objective optimization.

5.2. Qualitative Analysis

(1) Selection of the Globally Optimal working Mode for RMS

As seen with respect to the RMS expression in Table 12, the optimization algorithm was used to compare the RMS values of modes 1.1 and 1.4 in the low-power section, that is, $0 < P < k^2\ (1 - k)$.

Table 12. Expressions of RMS current for four locally optimal working modes in different power ranges.

$-k/2 < P < -k/3$	$-k/3 < P < k^2(k-1)$	$k^2(k-1) < P < 0$	$0 < P < k^2(1-k)$	$k^2(1-k) < P < k/3$	$k/3 < P < k/2$
	2.1 High-power range $I^2{}_{rms2.1} = I^2_{rms} = \frac{4}{3}kD_a^3 - \frac{2}{3}D_a^3 + 2kD_a^2D_{y2} - D_a^2 + 2kD_aD_{y2}^2 - 2kD_aD_{y2} - \frac{2}{3}k^2D_{y2}^3 + \frac{4}{3}kD_{y2}^3 + k^2D_{y2}^2 - 2kD_{y2}^2 + \frac{1}{3}$	2.1 Low-power range $I_{rms2.1} = \frac{2\sqrt{3}}{3}\sqrt{-\frac{P}{k}\sqrt{P(1-k)}}$	1.1 Low-power range $I_{rms1.1} = \frac{2\sqrt{3}}{3}\sqrt{\frac{P}{k}\sqrt{P(1-k)}}$	1.1 High-power range $I^2{}_{rms1.1} = I^2_{rms} = \frac{2}{3}k^2D_a^3 - \frac{4}{3}kD_a^3 + 2kD_a^2D_{y1} - k^2D_a^2 - 2kD_aD_{y1}^2 + 2kD_aD_{y1} + \frac{4}{3}kD_{y1}^3 - \frac{2}{3}D_{y1}^3 - 2kD_{y1}^2 + D_{y1}^2 + \frac{1}{3}k^2$	
2.3 High- and middle-power range $I^2{}_{rms2.3} = I^2_{rms} = \frac{8}{3}kD_a^3 - 4kD_a^2D_{y1} + 8kD_a^2 + 4kD_aD_{y1}^2 - 12kD_aD_{y1} + 8kD_a - \frac{4}{3}kD_{y1}^3 - \frac{2}{3}D_{y1}^3 + 6kD_{y1}^2 + D_{y1}^2 - 8kD_{y1} + \frac{1}{3}k^2 + \frac{8}{3}k$	2.3 Low-power range $I_{rms2.3} = \sqrt{\frac{1}{6} + \frac{1}{3}k^2 - \frac{1}{3}k - \sqrt{\frac{1}{4} + \frac{P}{k}}\left\|\left(\frac{1}{2} - k\right)\right\|\left(\frac{2}{3} - \frac{4}{3}\frac{P}{k}\right)}$	1.4 Low-power range $I_{rms1.4} = \sqrt{-\left\|\left(\frac{1}{2} - k\right)\right\|\left(\frac{2}{3} + \frac{4}{3}\frac{P}{k}\right)\sqrt{\frac{1}{4} - \frac{P}{k}} + \frac{1}{3}k^2 - \frac{1}{3}k + \frac{1}{6}}$	1.4 High- and middle-power range $I^2{}_{rms1.4} = I^2_{rms} = -\frac{8}{3}kD_a^3 + 4kD_a^2D_{y1} - 4kD_aD_{y1}^2 + 4kD_aD_{y1} + \frac{4}{3}kD_{y1}^3 - \frac{2}{3}D_{y1}^3 - 2kD_{y1}^2 + D_{y1}^2 + \frac{1}{3}k^2$	

Objective function:

$$min(I_{rms1.4} - I_{rms1.1}) = min(\sqrt{-\left|(\frac{1}{2} - k)\right|(\frac{2}{3} + \frac{4}{3}\frac{P}{k})\sqrt{\frac{1}{4} - \frac{p}{k}} + \frac{1}{3}k^2 - \frac{1}{3}k + \frac{1}{6}} - \frac{2\sqrt{3}}{3}\sqrt{\frac{P}{k}\sqrt{P(1-k)}}) \quad (36)$$

Constraints: $0 < k < 1$ and $0 < P < k^2(1 - k)$

By employing a single-objective genetic algorithm, we achieved $min(I_{\text{rms1.4}} - I_{\text{rms1.1}}) \geq 0$; then, we calculated $I_{\text{rms1.4}}$-$I_{\text{rms1.1}} \geq min(I_{\text{rms1.4}} - I_{\text{rms1.1}}) \geq 0$, where we obtained $I_{\text{rms1.4}} \geq I_{\text{rms1.1}}$. Therefore, in the low-power forward transmission range $0 < P < k^2(1-k)$, the current RMS value for mode 1.1 was lower than that for mode 1.4, making mode 1.1 the globally optimal solution.

Similarly, it can be proven from Table 12 and Appendix A—Tables A1 and A5—that we obtained the following results: in each mode power range and for different k values,

in the high- and middle-power section of forward transmission, the RMS value of mode 1.4 was lower than that of mode 1.1, so mode 1.4 was globally optimal. In the low-power section of reverse transmission, the RMS value of mode 2.1 was lower than that of mode 2.3, so mode 2.1 was the global optimum. In the high- and middle-power section, the RMS value of mode 2.3 was lower than that of mode 2.1, so mode 2.3 was the global optimum. From the above, the global optimal mode of the RMS value of different power segments in the full-power range was derived, as shown in Table 13.

Table 13. Global optimal modes of RMS in different power segments in full-power range.

Power Range	Reverse/High- and Middle-Power Range	Reverse/Low-Power Range	Forward/Low-Power Range	Forward/High- and Middle-Power Range
Global optimal operation mode	Mode 2.3	Mode 2.1	Mode 1.1	Mode 1.4

(2) The selection of the comprehensive global optimal mode and global optimal control variables.

Based on the globally optimal mode of stress from [19] and the globally optimal mode of the RMS value derived in the previous section, a comprehensive globally optimal mode in the full power range was obtained, as shown in Table 14. According to the above conclusions and the conclusions of stress optimization and RMS optimization in the local optimal mode in the previous section, the stress optimization control variables and RMS optimization control variables of the DAB converter in the full-power range were obtained, as shown in Table 15.

Table 14. Comprehensive global optimal modes of different power segments in full-power range.

Power Range	Reverse/High- and Middle-Power Range	Reverse/Low-Power Range	Forward/Low-Power Range	Forward/High- and Middle-Power Range
Global optimal operation mode	Mode 2.3	Mode 2.1	Mode 1.1	Mode 1.4

Table 15. Stress-optimal control variables and RMS value optimal control variables in full power range under DAB buck conditions.

Power Range	Stress-Optimal Control Variables	Power Range	RMS-Optimal Control Variables
2.3 High-power range $-\frac{k}{2} < P < k^2(k-1)$	$D_{y1} = 1 + (2k-2)\frac{\sqrt{\frac{1}{2}+\frac{P}{k}}}{\sqrt{(2k-1)^2+1}}$, $D_a = -\frac{1}{2} + (2k-1)\frac{\sqrt{\frac{1}{2}+\frac{P}{k}}}{\sqrt{(2k-1)^2+1}}$, $D_{y2} = 1$	2.3 High-power range $-k/2 < P < P_{linjie2.3}$	$D_{y1} = 1,\ D_a = -\frac{1-\sqrt{1-2\lvert P\rvert}}{2},\ D_{y2} = 1$
		Critical power $p_{linjie2.3}$	$D_{y1} = 1,\ D_a = -\frac{1-\sqrt{1-2\lvert P\rvert}}{2},\ D_{y2} = 1$ $k^3 + 2k^2P + (P^2-1)k - 2P = 0 \Rightarrow p_{linjie2.3}$
		2.3 Middle-power range $P_{linjie2.3} < P < k^2(k-1)$	$\frac{\partial I_{rms}^2}{\partial \theta} = (4b^2 - 4b^2k)cos^3\theta - 2b + (k - cos^2\theta(4b^2k + 4b^2) + 2b^2)sin\theta + 4bcos^2\theta + (4kb^2 - k - 2b^2)cos\theta = 0 \Rightarrow \theta$ θ may have multiple solutions, and the unique solution of θ is determined based on the minimum value constraint condition $b = \sqrt{\frac{1}{2}+\frac{P}{k}},\ D_a = -\frac{1}{2} + b\cos\theta, D_{y1} = 1 + b\cos\theta - b\sin\theta,\ D_{y2} = 1$
Critical power $P = k^2(k-1)$	$D_{y1} = k, D_a = k-1,\ D_{y2} = 1$		
2.1 Low-power range $k^2(k-1) < P < 0$	$D_{y1} = \sqrt{\frac{P}{k-1}}, D_a = -\frac{1}{k}\sqrt{P(k-1)},\ D_{y2} = \frac{1}{k}\sqrt{\frac{P}{k-1}}$		
1.1 Low-power range $0 < P < k^2(1-k)$	$D_{y1} = \sqrt{\frac{P}{1-k}},\ D_a = 0,\ D_{y2} = \frac{1}{k}\sqrt{\frac{P}{1-k}}$		
Critical power $P = k^2(1-k)$	$D_{y1} = k, D_a = 0,\ D_{y2} = 1$		
1.4 High-power range $k^2(1-k) < P < \frac{k}{2}$	$D_{y1} = 1 - (1-k)\frac{\sqrt{1-\frac{2P}{k}}}{\sqrt{(1-k)^2+k^2}}$, $D_a = \frac{1}{2} - \frac{1}{2}\frac{\sqrt{1-\frac{2P}{k}}}{\sqrt{(1-k)^2+k^2}}, D_{y2} = 1$	1.4 Middle-power range $k^2(1-k) < P < P_{linjie1.4}$	$\frac{\partial I_{rms}^2}{\partial \theta} = (2kcos^2\theta - 6cos\theta sin\theta - 4ksin^2\theta + k)b^2 + 6bsin\theta - 3k = 0. \Rightarrow \theta$ θ may have multiple solutions, and the unique solution of θ is determined based on the minimum value constraint condition $b = \sqrt{1-\frac{2P}{k}},\ D_{y1} = 1 - b\cos\theta, D_{y2} = 1,\ D_a = \frac{1}{2}(1 - b\cos\theta - b\sin\theta)$
		Critical power $P_{linjie1.4}$	$D_{y1} = 1,\ D_a = \frac{1-\sqrt{1-2P}}{2},\ D_{y2} = 1$ $k^3 - 2k^2P + (P^2-1)k + 2P = 0 \Rightarrow P_{linjie1.4}$
		1.4 High-power range $P_{linjie1.4} < P < k/2$	$D_{y1} = 1,\ D_a = \frac{1-\sqrt{1-2P}}{2},\ D_{y2} = 1$

6. Experimental Verification

6.1. Control Strategy

The relevant experimental parameters for the DAB are listed in Table 16. The proposed control strategies for stress optimization or RMS optimization in this paper are shown in

Figure 10. Based on Table 15, the regularities of the stress optimization variables and the regularities of the RMS optimization variables with different k values and different power ranges are presented in Figure 11.

Table 16. Experiment parameters of DAB converter.

Parameter	Value
Input port Voltage /V	200
Output port Voltage/V	80–200
Switching Frequency/Hz	5000
Transformer Turns Ratio	1:1
Additional Inductance/mH	1
Switching devices/IGBT	1KW50N60DTP
Controller	TMS320F28335

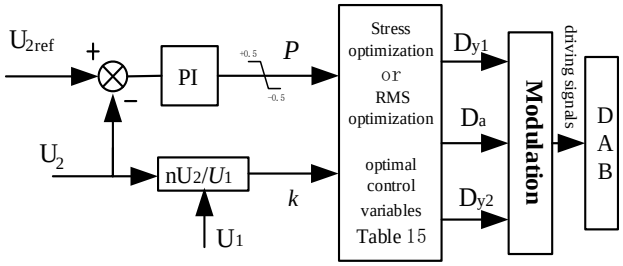


Figure 10. Stress or RMS optimization control strategy.

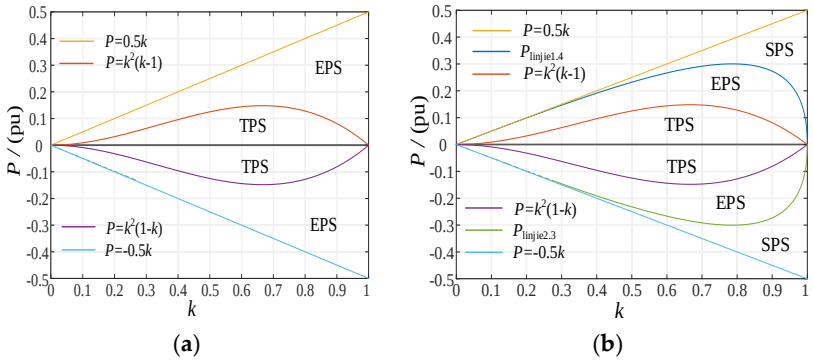


Figure 11. The regularity between stress optimization variables and the regularity between RMS optimization variables under different k and P. (**a**) Stress optimization. (**b**) RMS optimization.

6.2. Verification of the Effects of Unoptimized and Optimized Control Strategies

This section analyzes and compares the current stress and RMS values of the stress optimization control, RMS optimization control, and SPS control in the full-power range, as shown in Figure 12. As shown in Figure 12, at corresponding transmission power points, the current stress and RMS values under stress optimization control and RMS optimization control were not higher than those under SPS control. The smaller the transmission power in the positive and negative transmission directions was, the better the optimization effect of stress optimization control and RMS optimization control compared to SPS control. Compared to the optimization effect in the high-power range, the optimization effect in the low-power range was more significant. The stress optimization control and RMS optimization control overlap in the low-power segment, whereas they do not overlap in the high-power segment, but the optimization effects are close.

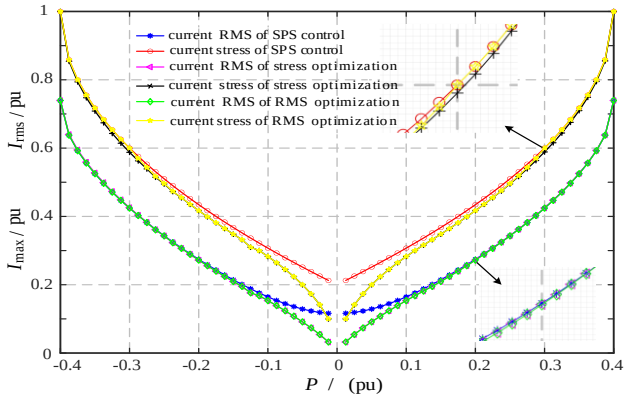
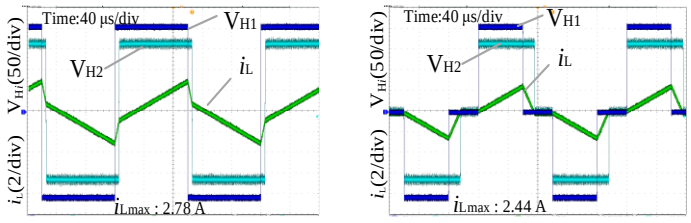


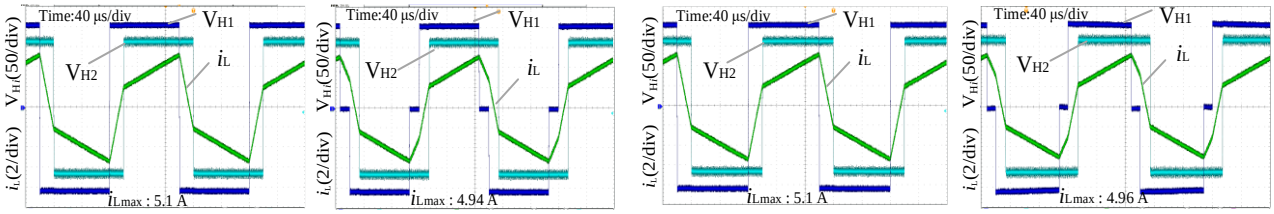
Figure 12. Comparison of current stress and RMS value for SPS, stress single-objective optimization, and RMS value single-objective optimization.

This paper further compares the stress optimization, RMS optimization, and SPS control at four power points in both low- and high-power segments for both forward and reverse transmission directions through experimental platforms, as shown in Figures 13 and 14 and Table 17.



(**a**) (**b**)

Figure 13. The comparison between nonoptimized and stress (RMS)-optimized: P = 0.075 (pu). (**a**) SPS control. (**b**) Stress or RMS optimization.



(**a**) (**b**) (**c**) (**d**)

Figure 14. The comparison between nonoptimized and stress-optimized: P = 0.25 (pu). (**a**) SPS control (**b**) Stress optimization. (**c**) SPS control. (**d**) RMS optimization.

Table 17. Comparison of unoptimized and optimized under different power.

P/(pu)	SPS Control	Stress Optimization	RMS Optimization
	Stress/RMS(A)	Stress/RMS (A)	Stress/RMS(A)
0.075	2.78/1.44	2.44/1.24	2.44/1.24
0.25	5.1/3.44	4.94 /3.43	4.96/3.43
−0.05	2.52/1.29	2/0.91	2/0.91
−0.3	6/4.24	5.88/4.26	6/4.24

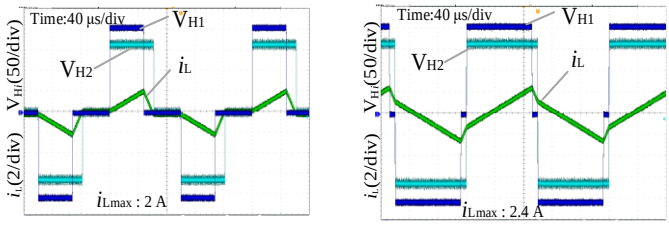
As shown in Figures 13 and 14 and Table 17, at the forward low-power point where P is 0.075 (pu), the optimization effects of stress optimization and RMS optimization

are identical, and both exhibited significantly better performance compared to the SPS control (unoptimized). At the forward high-power point where P is 0.25 (pu), the stress optimization and RMS optimization show slightly better optimization effects compared to the SPS control, but the differences are not substantial. The results of stress optimization and RMS optimization are very close.

As shown in Appendix A, Figures A1 and A2, at the reverse low-power point where P is −0.05 (pu), the effects of the stress optimization and RMS optimization are identical, and both resulted in significantly lower stress and RMS values compared to the unoptimized case. At the reverse high-power point where P is −0.3 (pu), the stress under stress optimization is lower than that under SPS control, while the RMS optimization and SPS control produced the same optimization results. In summary, it can be concluded that stress optimization and RMS optimization are more effective than SPS control optimization in the entire power range, and the optimization effect is more significant in the low-power range in particular. This conclusion is consistent with the theoretical analysis presented in the previous section.

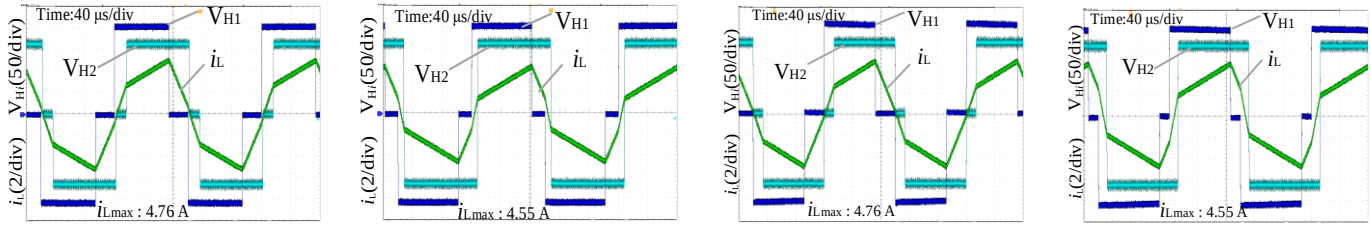
6.3. Comparison of Stress Optimization and RMS Value Optimization Among Different Local Optimal Modes

Under the control strategies of stress optimization and RMS optimization, the optimization effects of two locally optimal modes under the condition of overlapping transmission power have been compared to determine the globally optimal operating mode for this power point. This paper conducts comparisons on an experimental platform for two power points in the low- and high-power segments in the forward transmission direction, as shown in Figures 15 and 16.



(**a**) (**b**)

Figure 15. Stress optimization (RMS optimization) comparison for mode 1.1 and 1.4, where P = 0.225 (pu). (**a**) Mode 1.1. (**b**) Mode 1.4.



(**a**) (**b**) (**c**) (**d**)

Figure 16. Stress optimization comparison and RMS optimization comparison for mode 1.1 and 1.4, where P = 0.225 (pu). (**a**) Stress optimization in mode 1.1. (**b**) Stress optimization in mode 1.4. (**c**) RMS optimization in mode 1.1. (**d**) RMS optimization in mode 1.4.

As shown in Figure 15 and Table 18, The current stress and RMS values for mode 1.1 and mode 1.4 at a low power P of 0.05 (pu) under forward transmission are presented. In the low-power segment, the optimization results for stress optimization and RMS optimization are identical. Under both optimization methods, mode 1.1 showed better optimization

effects than mode 1.4. At this low-power point, mode 1.1 was deemed the globally optimal mode.

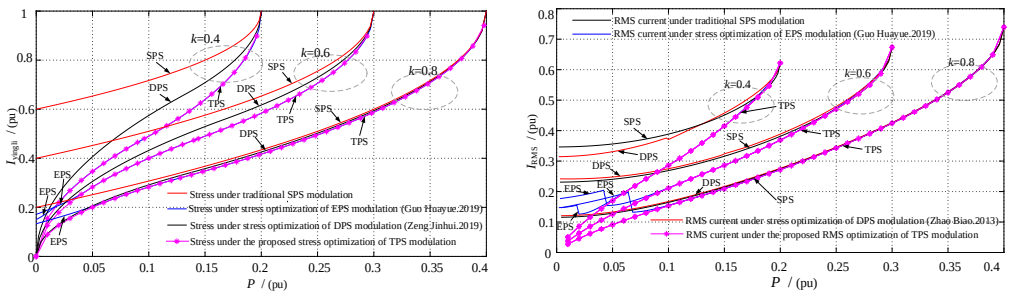
Table 18. Comparison of stress optimization and comparison of RMS optimization of different local optimal modes.

P/(pu)	Mode 1.1	Mode 1.4	The Globally Optimal Mode
	Stress/RMS (A)	Stress/RMS (A)	
		Stress optimization	
0.05	2/0.91	2.4/1.26	Mode 1.1
0.225	4.76/3.21	4.55/3.07	Mode 1.4
		RMS optimization	
0.05	2/0.91	2.4/1.26	Mode 1.1
0.225	4.76/3.21	4.55/3.06	Mode 1.4

As shown in Figure 16 and Table 18, the stress optimization and RMS optimization results for mode 1.1 and mode 1.4 at a high power *P* of 0.225 (pu) under forward transmission are presented. The optimization results for stress optimization and RMS optimization differ, but in both optimization methods, mode 1.4 exhibited better optimization effects than mode 1.1. At this high-power point, mode 1.4 was the globally optimal mode. These experimental results are consistent with the theoretical analysis of stress optimization and RMS optimization presented in the previous section.

6.4. Comparison of Stress Optimization and RMS Optimization Under Different Modulation Strategies

In this section, the stress optimization comparison and RMS optimization comparison of k = 0.4, 0.6, and 0.8 under different modulation strategies have been conducted by a MATLAB program, as shown in Figure 17. From Figure 17a, it can be observed that the stress under stress optimization with TPS modulation is not higher than that with other modulation strategies. In the high-power segment, the stress under stress optimization with TPS modulation is the same as that with EPS modulation, aligning with the conclusion presented in Section 4 of this paper. For the low-power segment, the stress under stress optimization with TPS modulation is lower than that with EPS modulation. For low-transmission power segments or voltage mismatch conditions, stress optimization under TPS modulation demonstrates superior optimization effects compared to other modulation strategies.



(**a**) (**b**)

Figure 17. The comparison under different modulation strategies for k = 0.4, 0.6, and 0.8. (**a**) Stress comparison of stress optimization, where EPS: (Guo Huayue 2019) from Ref. [6], DPS: (Zeng Jinhui 2019) from Ref. [7]. (**b**) RMS current comparison of RMS optimization and stress optimization, where EPS: (Guo Huayue 2019) from Ref. [6], DPS: (Zhao Biao 2013) from Ref. [14].

As shown in Figure 17b, under RMS optimization, the RMS value with TPS modulation is not higher than that with other modulation strategies. The RMS value under RMS

optimization with TPS modulation is the same as that with SPS modulation in the high-power segment; it is very close to the stress optimization under EPS modulation in the medium-power segment; it is lower than the RMS values under stress optimization with other modulations in the low-power segment. These findings align with the conclusions presented in the fourth section. For low transmission power segments or voltage mismatch conditions, RMS optimization under TPS modulation exhibits better optimization effects than other modulation strategies.

6.5. Efficiency Comparison Using Stress Optimization Control, RMS Optimization Control, and SPS Control

The experimental platform was used to compare the efficiency of current stress optimization control, RMS optimization control, and SPS control for different transmission power levels at k = 0.4, 0.6, and 0.8, as shown in Figure 18. As is evident from Figure 18, the current stress value optimization and RMS optimization of TPS were more efficient than SPS across the entire power range, with a greater advantage in the low-power segment. Moreover, the greater the degree of voltage mismatch (representing a smaller k value), the more obvious the optimization effect of current stress or RMS value modulated by TPS ended up being.

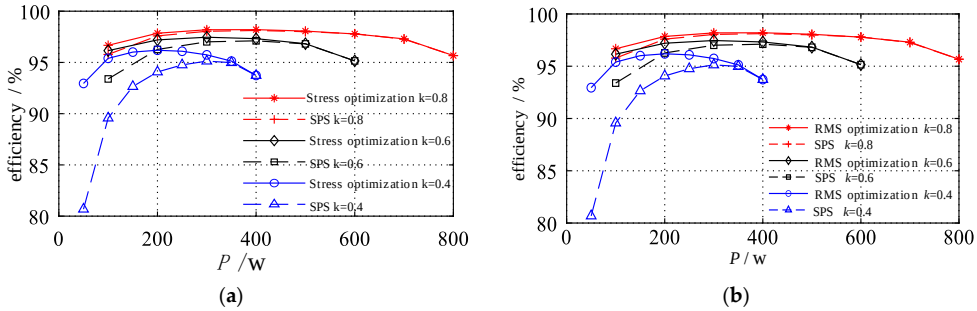


Figure 18. Comparison of the efficiency of the two optimization methods and SPS for k = 0.4, 0.6, and 0.8. (**a**) Comparison of the efficiency of stress optimization and SPS. (**b**) Comparison of the efficiency of RMS optimization and SPS.

7. Conclusions

This paper studied the regularities among the optimization variables in different power segments of three optimizations in four local optimal modes, analyzed the inherent relationships and connections of the three optimizations, and derived the corresponding optimized control variables based on the regularities among the optimization variables. Finally, by comparing the stress and RMS values of different locally optimal modes, the globally optimal operating mode and globally optimized control variables were determined. Based on theoretical research and experimental verification, the following conclusions are drawn:

(1) This paper derived the globally optimal control variables for the current RMS in the full power range, enabling real-time optimized control under the fluctuation of power P or transformation ratio k. The optimization strategy showed more significant efficiency improvements under the condition of low-power section and voltage mismatch at both ends.

(2) Three optimization results of different local optimal modes were obtained via optimization algorithms and then compared and analyzed: The optimization regularities and optimization results of the two optimizations in mode 1.1 and 2.1 are the same. In these modes, the minimum stress and the minimum RMS value are the same point. The optimization regularities and optimization results of the three optimizations in modes 1.4 and 2.3 are the same in the low-power section. In these modes, the minimum stress and the minimum RMS value in the low power section are the same point. However, in the high-power section, the optimization regularities and optimization

results are different: the minimum stress and the minimum RMS value are not the same point.

(3) By selecting the globally optimal control variables for stress or RMS value across different modes and power segments, we can draw the following conclusions: Under stress optimization, the optimal control in the low-power segment is actually TPS modulation control, while in the high-power segment, the optimal control is EPS modulation control. Under RMS optimization, the optimal control in the low-power segment is TPS modulation control; in the medium-power segment, it is EPS modulation control; in the high-power segment, it is SPS modulation control.

Author Contributions: Writing—original draft, L.Z.; Writing—review & editing, C.T., F.X., B.L. and P.L. All authors have read and agreed to the published version of the manuscript.

Funding: This research was funded by National Natural Science Foundation of China, grant number 52130704.

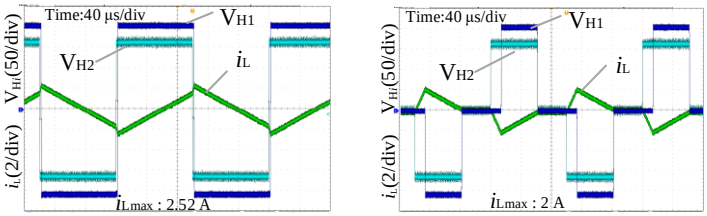
Data Availability Statement: The original contributions presented in this study are included in the article. Further inquiries can be directed to the corresponding author.

Conflicts of Interest: The authors declare no conflict of interest.

Appendix A

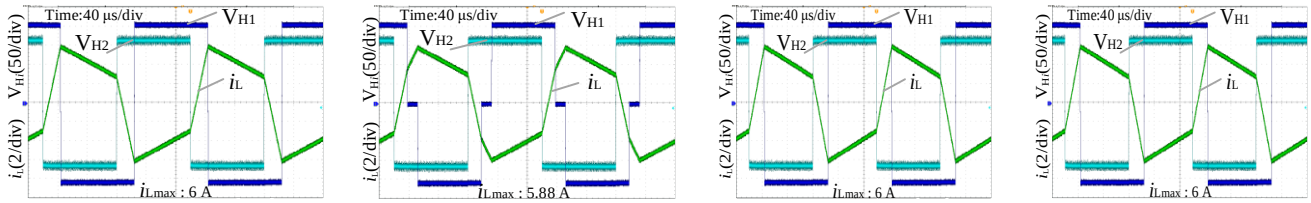
Table A1. The RMS variable regularity and RMS optimal control variables of DAB in different power sections in the full-power range of three working modes under buck conditions.

$k<1$	Power Range	Variable Regularity	RMS-Optimal Control Parameters and the Minimum RMS Value
Mode 1.1 $p>0$	Low-power range $0<P<k^2(1-k)$	$\begin{cases} D_{y1}=kD_{y2} \\ D_a=0 \end{cases}$	$D_{y2}=\frac{1}{k}\sqrt{\frac{P}{1-k}},\ D_{y1}=\sqrt{\frac{P}{1-k}},\ D_a=0,\ I_{rms_min}=\frac{2\sqrt{3}}{3}\sqrt{\frac{P}{k}\sqrt{P(1-k)}}$
	Critical power $p=k^2(1-k)$		$D_{y1}=k, D_a=0, D_{y2}=1,\ I_{rms_min}=\frac{2\sqrt{3}}{3}k(1-k)$
	High-power range $k^2(1-k)<P<k/2$	$D_a+D_{y2}=1$	$\frac{\partial I_{Frms}^2}{\partial\theta}=\frac{2}{27}b[(-3\sqrt{3}bk^2+6\sqrt{3}bk)cos(2\theta)+(6\sqrt{3}b^2k^2-6\sqrt{3}b^2k+6\sqrt{3}b^2)sin(3\theta)+$ $(9b^2k^2-18b^2k-6k^2+12k)cos\theta+(-3bk^2-6bk+6b)sin(2\theta)+(-3\sqrt{3}b^2k^2$ $-6\sqrt{3}b^2k+6\sqrt{3}b^2+2\sqrt{3}k^2+4\sqrt{3}k-4\sqrt{3})sin\theta]=0\Rightarrow\ \theta$ θ may have multiple solutions, and the unique solution of θ is determined based on the minimum value constraint condition, which is then substituted into the trigonometric function in the polar coordinates. $let: b^2=\frac{1}{3}-\frac{P}{k},\ b^2=(D_a-\frac{1}{2}D_{y1})^2+\frac{3}{4}(D_{y1}-\frac{2}{3})^2\Rightarrow D_{y1}=\frac{2}{3}+\frac{2\sqrt{3}}{3}b\cos\theta, D_a=\frac{1}{3}+\frac{\sqrt{3}}{3}b\cos\theta+b\sin\theta$ $I_{rms}^2=-\frac{4}{3}kD_a^3+4kD_{y1}D_a^2-4kD_aD_{y1}^2+4kD_aD_{y1}D_{y2}+\frac{4}{3}kD_{y1}^3-\frac{2}{3}D_{y1}^3-2kD_{y1}^2D_{y2}+D_{y1}^2$ $+2kD_{y1}D_{y2}^2-2kD_{y1}D_{y2}-\frac{2}{3}k^2D_{y2}^3+k^2D_{y2}^2$
Mode 2.1 $p<0$	Low-power range $k^2(k-1)<P<0$	$\begin{cases} D_{y1}=kD_{y2} \\ D_{y1}-D_a=D_{y2} \end{cases}$	$D_{y1}=\sqrt{\frac{P}{k-1}}, D_{y2}=\frac{1}{k}\sqrt{\frac{P}{k-1}},\ D_a=-\frac{1}{k}\sqrt{P(k-1)}, I_{rms_min}=\sqrt{-\frac{4P}{3k}\sqrt{P(k-1)}}$
	Critical power $P=k^2(k-1)$		$D_{y1}=k, D_a=k-1, D_{y2}=1\ I_{rms_min}=\frac{2\sqrt{3}}{3}k(1-k)$
	High-power range $-k/3<P<k^2(k-1)$	$D_{y1}-D_a=1$	$\frac{\partial I_{rms}^2}{\partial\theta}=(6\sqrt{3}k^2b^2-6\sqrt{3}kb^2+6\sqrt{3}b^2)cos(3\theta)+(12k-18b^2k+9b^2-6)sin\theta+(-6bk^2+6bk+3b)sin(2\theta)$ $+(3\sqrt{3}b-6\sqrt{3}bk)cos(2\theta)+(-6\sqrt{3}k^2b^2+6\sqrt{3}kb^2+3\sqrt{3}b^2+4\sqrt{3}k^2-4\sqrt{3}k-2\sqrt{3})cos\theta=0\Rightarrow\ \theta$ θ may have multiple solutions, and the unique solution of θ is determined based on the minimum value constraint condition, which is then substituted into the trigonometric function in the polar coordinates. $let: b^2=\frac{1}{3}+\frac{P}{k},\ b^2=(D_a+\frac{1}{2}D_{y2})^2+\frac{3}{4}(D_{y2}-\frac{2}{3})^2\Rightarrow D_{y2}=\frac{2}{3}+\frac{2\sqrt{3}}{3}b\sin\theta,\ D_a=-\frac{1}{3}-\frac{\sqrt{3}}{3}b\sin\theta+b\cos\theta$ $I_{rms}^2=\frac{4}{3}kD_a^3-\frac{2}{3}D_a^3+2kD_a^2D_{y2}-D_a^2+2kD_aD_{y2}^2-2kD_aD_{y2}-\frac{2}{3}k^2D_{y2}^3+\frac{4}{3}kD_{y2}^3+k^2D_{y2}^2-2kD_{y2}^2+\frac{1}{3}$
Mode 2.3 $p<0$	Low-power range $k^2(k-1)<P<0$	$\begin{cases} D_{y1}-D_a=1 \\ D_{y2}=1 \end{cases}$	$k\le 0.5: D_{y1}=-\sqrt{\frac{1}{4}+\frac{P}{k}+\frac{1}{2}}, D_a=-\sqrt{\frac{1}{4}+\frac{P}{k}-\frac{1}{2}}, D_{y2}=1\ I_{rms_min}=$ $\sqrt{\frac{1}{6}+\frac{1}{3}k^2-\frac{1}{3}k-\sqrt{\frac{P}{k}+\frac{1}{4}}(\frac{1}{2}-k)(\frac{2}{3}-\frac{4}{3}\frac{P}{k})}$ $k>0.5: D_{y1}=\sqrt{\frac{1}{4}+\frac{P}{k}}+\frac{1}{2}, D_a=\sqrt{\frac{1}{4}+\frac{P}{k}}-\frac{1}{2}, D_{y2}=1, I_{rms_min}=$ $\sqrt{\frac{1}{6}+\frac{1}{3}k^2-\frac{1}{3}k+\sqrt{\frac{P}{k}+\frac{1}{4}}(\frac{1}{2}-k)(\frac{2}{3}-\frac{4}{3}\frac{P}{k})}$
	Critical power $P=k^2(k-1)$		$D_{y1}=k, D_a=k-1, D_{y2}=1,\ I_{rms_min}=\frac{2\sqrt{3}}{3}k(1-k)$
	Middle-power range $P_linjie2.3<P$ $<k^2(k-1)$	$D_{y2}=1$	$\frac{\partial I_{rms}^2}{\partial\theta}=(4b^2-4b^2k)cos^3\theta-2b+(k-cos^2\theta(4b^2k+4b^2)+2b^2)sin\theta+4bcos^2\theta+(4kb^2-k-2b^2)cos\theta=0\ \Rightarrow\ \theta$ θ may have multiple solutions, and the unique solution of θ is determined based on the minimum value constraint condition, which is then substituted into the trigonometric function in polar coordinates. $let: b^2=\frac{1}{2}+\frac{P}{k}, b^2=(D_a+\frac{1}{2})^2+\left[D_{y1}-(D_a+\frac{3}{2})\right]^2\Rightarrow D_{y1}=1+b\cos\theta-b\sin\theta,\ D_a=-\frac{1}{2}+b\cos\theta$ $I_{rms}^2=$ $\frac{8}{3}kD_a^3-4kD_a^2D_{y1}+8kD_a^2+4kD_aD_{y1}^2-12kD_aD_{y1}+8kD_a-\frac{4}{3}kD_{y1}^3-\frac{2}{3}D_{y1}^3+6kD_{y1}^2+D_{y1}^2-8kD_{y1}+\frac{1}{3}k^2+\frac{8}{3}k$
	Critical power $P_linjie2.3$		$D_{y1}=1, D_{y2}=1, D_a=-\frac{1-\sqrt{1-2|P|}}{2}\ I_{rms_min}=\sqrt{-\frac{2}{3}k(1+2P)^{\frac{1}{2}}(1-P)+\frac{1}{3}k^2+\frac{1}{3}}$ $k^3+2k^2P+(p^2-1)k-2P=0\Rightarrow p_linjie2.3$
	High-power range $-\frac{k}{2}<P<P_linjie2.3$	$\begin{cases} D_{y1}=1 \\ D_{y2}=1 \end{cases}$	$D_{y1}=1, D_{y2}=1, D_a=-\frac{1-\sqrt{1-2|P|}}{2}\ I_{rms_min}=\sqrt{-\frac{2}{3}k(1+2P)^{\frac{1}{2}}(1-P)+\frac{1}{3}k^2+\frac{1}{3}}$



(**a**) (**b**)

Figure A1. The comparison between nonoptimized and stress (RMS value)-optimized: $P = -0.05$. (**a**) SPS control. (**b**) Stress or RMS optimization.



(**a**) (**b**) (**c**) (**d**)

Figure A2. The comparison between nonoptimized and stress-optimized: $P = -0.3$. (**a**) SPS control. (**b**) Stress optimization. (**c**) SPS control. (**d**) RMS optimization.

Table A2. The trigonometric polar coordinate method in the high-power segments of working modes 1.1, 2.1, and 2.3.

Mode 1.1	A Trigonometric Function Polar Coordinate	Mode 2.1	A Trigonometric Function Polar Coordinate	Mode 2.3	A Trigonometric Function Polar Coordinate
Variable regularity $D_{y2} + D_a = 1$	$P = -k(D_a{}^2 - 2D_a D_{y1} + D_{y1}{}^2 - D_{y2} D_{y1})$ $\frac{1}{3} - \frac{P}{k} = (D_a - \frac{1}{2} D_{y1})^2 + \frac{3}{4}(D_{y1} - \frac{2}{3})^2$ let$b^2 = \frac{1}{3} - \frac{P}{k}$ $b^2 = (D_a - \frac{1}{2} D_{y1})^2 + \frac{3}{4}(D_{y1} - \frac{2}{3})^2$ $\begin{cases} D_{y1} = \frac{2}{3} + \frac{2\sqrt{3}}{3} b\cos\theta \\ D_a = \frac{1}{3} + \frac{\sqrt{3}}{3} b\cos\theta + b\sin\theta \end{cases}$	Variable regularity $D_{y1} - D_a = 1$	$P = k(D_a{}^2 + D_a D_{y2} + D_{y2}{}^2 - D_{y2})$ $\frac{1}{3} + \frac{P}{k} = (D_a + \frac{1}{2} D_{y2})^2 + \frac{3}{4}(D_{y2} - \frac{2}{3})^2$ let : $b^2 = \frac{1}{3} + \frac{P}{k}$ $b^2 = (D_a + \frac{1}{2} D_{y2})^2 + \frac{3}{4}(D_{y2} - \frac{2}{3})^2$ $\begin{cases} D_{y2} = \frac{2}{3} + \frac{2\sqrt{3}}{3} b\sin\theta \\ D_a = -\frac{1}{3} - \frac{\sqrt{3}}{3} b\sin\theta + b\cos\theta \end{cases}$	Variable regularity $D_{y2} = 1$	$P = k(2D_a{}^2 - 2D_a D_{y1} + 4D_a + D_{y1}{}^2 - 3D_{y1} + 2)$ $\frac{1}{2} + \frac{P}{k} = (D_a + \frac{1}{2})^2 + \left[D_{y1} - (D_a + \frac{3}{2})\right]^2$ let : $b^2 = \frac{1}{2} + \frac{P}{k}$ $b^2 = (D_a + \frac{1}{2})^2 + \left[D_{y1} - (D_a + \frac{3}{2})\right]^2$ $\begin{cases} D_{y1} = 1 + b\cos\theta - b\sin\theta \\ D_a = -\frac{1}{2} + b\cos\theta \end{cases}$

Table A3. The derivative of the square of the RMS current in high-power range for working modes 1.1, 1.4, 2.1, and 2.3.

Mode 1.1	I_{rms}^2	$I_{rms}^2 = -\frac{4}{3}kD_a^3 + 4kD_{y1}D_a^2 - 4kD_aD_{y1}^2 + 4kD_aD_{y1}D_{y2} + \frac{4}{3}kD_{y1}^3 - \frac{2}{3}D_{y1}^3$ $-2kD_{y1}^2D_{y2} + D_{y1}^2 + 2kD_{y1}D_{y2}^2 - 2kD_{y1}D_{y2} - \frac{2}{3}k^2D_{y2}^3 + k^2D_{y2}^2$
	$\frac{\partial^2(I_{rms}^2)}{\partial^2\theta}$	$\frac{\partial I_{rms}^2}{\partial\theta} = \frac{2}{27}b[(-3\sqrt{3}bk^2 + 6\sqrt{3}bk)cos(2\theta) + (6\sqrt{3}b^2k^2 - 6\sqrt{3}b^2k + 6\sqrt{3}b^2)sin(3\theta) + (9b^2k^2 - 18b^2k - 6k^2$ $+12k)cos\theta + (-3bk^2 - 6bk + 6b)sin(2\theta) + (-3\sqrt{3}b^2k^2 - 6\sqrt{3}b^2k + 6\sqrt{3}b^2 + 2\sqrt{3}k^2 + 4\sqrt{3}k - 4\sqrt{3})sin\theta] = 0$
	$\frac{\partial^2(I_{rms}^2)}{\partial\theta^2}$	$\frac{\partial^2(I_{rms}^2)}{\partial\theta^2} = \frac{2}{27}b[(18\sqrt{3}b^2k^2 - 18\sqrt{3}b^2k + 18\sqrt{3}b^2)cos(3\theta) + (6\sqrt{3}bk^2 - 12\sqrt{3}bk)sin(2\theta) + (-6bk^2 - 12bk$ $+12b)cos(2\theta) + (-3\sqrt{3}b^2k^2 - 6\sqrt{3}b^2k + 6\sqrt{3}b^2 + 2\sqrt{3}k^2 + 4\sqrt{3}k - 4\sqrt{3})cos\theta + (-9b^2k^2 + 18b^2k + 6k^2 - 12k)sin\theta]$
Mode 2.1	I_{rms}^2	$I_{rms}^2 = \frac{4}{3}kD_a^3 + 4kD_a^2D_{y2} - 4kD_aD_{y1}D_{y2} + 4kD_aD_{y2}^2 - \frac{2}{3}D_{y1}^3 + 2kD_{y1}^2D_{y2}$ $+D_{y1}^2 - 2kD_{y1}D_{y2}^2 - 2kD_{y1}D_{y2} - \frac{2}{3}k^2D_{y2}^3 + \frac{4}{3}kD_{y2}^3 + k^2D_{y2}^2$
	$\frac{\partial^2(I_{rms}^2)}{\partial\theta^2}$	$\frac{\partial I_{rms}^2}{\partial\theta} = \frac{2}{27}b\left[\begin{array}{l}(6\sqrt{3}k^2b^2 - 6\sqrt{3}kb^2 + 6\sqrt{3}b^2)cos(3\theta) + (12k - 18b^2k + 9b^2 - 6)sin\theta + (-6bk^2 + 6bk + 3b)sin(2\theta) \\ +(3\sqrt{3}b - 6\sqrt{3}bk)cos(2\theta) + (-6\sqrt{3}k^2b^2 + 6\sqrt{3}kb^2 + 3\sqrt{3}b^2 + 4\sqrt{3}k^2 - 4\sqrt{3}k - 2\sqrt{3})cos\theta\end{array}\right]$
	$\frac{\partial^2(I_{rms}^2)}{\partial\theta^2}$	$\frac{\partial^2(I_{rms}^2)}{\partial\theta^2} = \frac{2}{27}b\left[\begin{array}{l}(-12bk^2 + 12bk + 6b)cos(2\theta) + (12\sqrt{3}bk - 6\sqrt{3}b)sin(2\theta) + (6\sqrt{3}b^2k^2 - 6\sqrt{3}b^2k - 3\sqrt{3}b^2 - 4\sqrt{3}k^2 \\ +4\sqrt{3}k + 2\sqrt{3})sin\theta + (12k - 18b^2k + 9b^2 - 6)cos\theta + (-18\sqrt{3}b^2k^2 + 18\sqrt{3}b^2k - 18\sqrt{3}b^2)sin(3\theta)\end{array}\right]$
Mode 2.3	I_{rms}^2	$I_{rms}^2 = \frac{8}{3}kD_a^3 - 4kD_a^2D_{y1} + 4kD_a^2D_{y2} + 4kD_a^2 + 4kD_aD_{y1}^2 - 4kD_aD_{y1}D_{y2} - 8kD_aD_{y1} + 4kD_aD_{y2}^2 + 4kD_a$ $-\frac{4}{3}kD_{y1}^3 - \frac{2}{3}D_{y1}^3 + 2kD_{y1}^2D_{y2} + 4kD_{y1}^2 + D_{y1}^2 - 2kD_{y1}D_{y2}^2 - 2kD_{y1}D_{y2} - 4kD_{y1} - \frac{2}{3}k^2D_{y2}^3 + \frac{4}{3}kD_{y2}^3 + k^2D_{y2}^2 + \frac{4}{3}k$
	$\frac{\partial^2(I_{rms}^2)}{\partial^2\theta}$	$\frac{\partial I_{rms}^2}{\partial\theta} = b\left[(4b^2 - 4b^2k)cos^3\theta - 2b + (k - cos^2\theta(4b^2k + 4b^2) + 2b^2)sin\theta + 4bcos^2\theta + (4kb^2 - k - 2b^2)cos\theta\right]$
	$\frac{\partial^2(I_{rms}^2)}{\partial\theta^2}$	$\frac{\partial^2(I_{rms}^2)}{\partial\theta^2} = b\left[(-3b^2k - 3b^2)cos(3\theta) + (k - b^2k + b^2)cos\theta + (3b^2k - 3b^2)sin(3\theta) - 4bsin(2\theta) + (k - b^2k - b^2)sin\theta\right]$

Table A4. Node current of different working modes.

Node Current	Mode 1.1	Mode 1.4	Mode 2.1	Mode 2.3
I_0	$-(D_{y1}-kD_{y2})$	$-(D_{y1}-2k+2kD_a+kD_{y2})$	$2kD_a-D_{y1}+kD_{y2}$	$2kD_a-D_{y1}+kD_{y2}$
I_1	$2D_a-D_{y1}+kD_{y2}$	$2D_a-D_{y1}+2D_{y2}+kD_{y2}-2$	$2D_a-D_{y1}+2D_{y2}-kD_{y2}$	$2D_a-D_{y1}+2D_{y2}-kD_{y2}$
I_2	$D_{y1}+2kD_a-2kD_{y1}+kD_{y2}$	$2D_a-D_{y1}+kD_{y2}$	$D_{y1}-kD_{y2}$	$2D_a-D_{y1}-kD_{y2}+2$
I_3	$D_{y1}-kD_{y2}$	$D_{y1}+2kD_a-2kD_{y1}+kD_{y2}$	$D_{y1}-kD_{y2}$	$-(2k-D_{y1}+2kD_a-2kD_{y1}+kD_{y2})$

Table A5. Using genetic algorithm to compare the RMS current of different locally optimal modes in different power ranges.

Power Range	Forward/High- and Middle-Power Range: $k^2(1-k)<P<k/3$	Reverse/Low-Power Range: $k^2(k-1)<P<0$	Reverse/High- and Middle-Power Range: $-k/3<P<k^2(k-1)$
Objective function	$\min(I^2_{rms1.1}-I^2_{rms1.4})$ $I^2_{rms1.1}$ and $I^2_{rms1.4}$ from Table 12, 15 and A1 high power range of mode	$\min(I_{rms2.3}-I_{rms2.1})$ $=\min(\sqrt{\frac{1}{6}+\frac{1}{3}k^2-\frac{1}{3}k}-\sqrt{\frac{1}{4}+\frac{P}{k}}\left\|(\frac{1}{2}-k)\right\|(\frac{2}{3}-\frac{4}{3}\frac{P}{k})$ $-\frac{2\sqrt{3}}{3}\sqrt{-\frac{P}{k}\sqrt{P(1-k)}})$	$\min(I^2_{rms2.1}-I^2_{rms2.3})$ $I^2_{rms2.1}$ and $I^2_{rms2.3}$ from Tables 12 and A1 high power range of mode
Constraints	$0<k<1, k^2(1-k)<P<k/3$	$0<k<1, k^2(k-1)<P<0$	$0<k<1, -k/3<P<k^2(k-1)$
Result	$min(I^2_{\mathrm{rms1.1}}-I^2_{\mathrm{rms1.4}})\geq 0$	$min(I_{\mathrm{rms2.3}}-I_{\mathrm{rms2.1}})\geq 0,$	$min(I^2_{\mathrm{rms2.1}}-I^2_{\mathrm{rms2.3}})\geq 0,$

References

1. Zhao, B.; An, F.; Song, Q. Development and Application of DC Transformer Based on Dual-active-bridge. *Proc. CSEE* **2021**, *41*, 288–298. (In Chinese)
2. Lin, C.; Ge, X.; Wang, H. Low-Frequency Stability Analysis of Train-Grid System: A Perspective From DAB Converter. *IEEE Trans. Power Electron.* **2024**, *39*, 9066–9071. [CrossRef]
3. Meng, X.; Hu, G.; Liu, Z.; Wang, H.; Zhang, G. Neural Network-Based lmpedance ldentification and Stability Analysis for Double-Sided Feeding Railway Systems. *IEEE Trans. Transp. Electrif.* **2024**. [CrossRef]
4. Zhao, B.; Song, Q.; Liu, W. Overview of dual-active-bridge isolated bidirectional DC–DC converter for high-frequency-link power-conversion system. *IEEE Trans. Power Electron.* **2014**, *29*, 4091–4106. [CrossRef]
5. Gu, Q.; Yuan, L.; Nie, J. Current stress minimization of dual-active-bridge DC–DC converter within the whole operating range. *IEEE J. Emerg. Sel. Top. Power Electron.* **2019**, *7*, 129–142. [CrossRef]
6. Guo, H.; Zhang, X.; Zhao, W. Optimal control strategy of dual active bridge DC-DC converters with extended-phase-shift control. *Proc. CSEE* **2019**, *39*, 3889–3898. (In Chinese)
7. Zeng, J.; Sun, Z.; Lei, M. Global current stress analysis and optimal control strategy of dual-active full bridge converter based on dual phase shift control. *Trans. China Electrotech. Society* **2019**, *34*, 2507–2518. (In Chinese)
8. Li, J.; Luo, Q.; Mou, D. A Hybrid Five-Variable Modulation Scheme for Dual-Active-Bridge Converter With Minimal RMS Current. *IEEE Trans. Ind. Electron.* **2022**, *69*, 336–346. [CrossRef]
9. Mou, D.; Luo, Q.; Li, J. Five-Degree-of-Freedom Modulation Scheme for Dual Active Bridge DC–DC Converter. *IEEE Trans. Power Electron.* **2021**, *36*, 10584–10601. [CrossRef]
10. Shao, S.; Jiang, M.; Ye, W.; Li, Y. Optimal Phase-Shift Control to Minimize Reactive Power for a Dual Active Bridge DC–DC Converter. *IEEE Trans. Power Electron.* **2019**, *34*, 10193–10205. [CrossRef]
11. Hou, N.; Zhang, Y.; Li, Y.W. A Natural Transient-Behavior-Based Control Theory for DAB-Based Two-Stage DC-DC Converter. *IEEE Trans. Power Electron.* **2023**, *38*, 15137–15141. [CrossRef]
12. Shao, S.; Chen, L.; Shan, Z.; Gao, F. Modeling and Advanced Control of Dual-Active-Bridge DC–DC Converters: A Review. *IEEE Trans. Power Electron.* **2022**, *37*, 1524–1547. [CrossRef]
13. Hu, Y.; Zhang, T.; Yang, L. Comparative Study of Reactive Power Optimization and Current Stress Optimization of DAB Converter with Dual Phase Shift Control. *Proc. CSEE* **2020**, *40*, 243–253. (In Chinese)
14. Zhao, B.; Song, Q.; Liu, W. Current stress-optimized switching strategy of isolated bidirectional DC-DC converter with dual-phase-shift control. *IEEE Trans. Ind. Electron.* **2013**, *60*, 4458–4467. [CrossRef]
15. Hebala, O.M.; Aboushady, A.A.; Ahmed, K.H. Generic Closed-Loop Controller for Power Regulation in Dual Active Bridge DC-DC Converter With Current Stress Minimization. *IEEE Trans. Ind. Electron.* **2019**, *66*, 4468–4478. [CrossRef]
16. Tong, A.; Hang, L.; Li, G.; Jiang, X. Modeling and analysis of a dual-active-bridge-isolated bidirectional DC/DC converter to minimize rms current with whole operating range. *IEEE Trans. Power Electron.* **2018**, *33*, 5302–5316. [CrossRef]
17. Huang, J.; Wang, Y.; Li, Z. Unified Triple-Phase-Shift Control to Minimize Current Stress and Achieve Full Soft-Switching of Isolated Bidirectional DC–DC Converter. *IEEE Trans. Ind. Electron.* **2016**, *63*, 4169–4179. [CrossRef]

18. Qiang, R.; Sheng, A. A three degree freedom optimal control strategy of dual-active-bridge converters for full range operations. *Proc. CSEE* **2020**, *40*, 3613–3621. (In Chinese)
19. Zhang, L.; Tu, C.; Xiao, F. Intrinsic Law Analysis and Optimization Control of Current Stress in Dual Active Bridge Converter. *Trans. China Electrotech. Soc.* **2024**. [CrossRef]

Disclaimer/Publisher's Note: The statements, opinions and data contained in all publications are solely those of the individual author(s) and contributor(s) and not of MDPI and/or the editor(s). MDPI and/or the editor(s) disclaim responsibility for any injury to people or property resulting from any ideas, methods, instructions or products referred to in the content.